

Rewiring endogenous genes in CAR T cells for tumour-restricted payload delivery

<https://doi.org/10.1038/s41586-025-09212-7>

Received: 14 December 2023

Accepted: 29 May 2025

Published online: 2 July 2025

Open access

 Check for updates

Amanda X. Y. Chen^{1,2,11} , Kah Min Yap^{1,2,11} , Joelle S. Kim^{1,2}, Kevin Sek^{1,2}, Yu-Kuan Huang^{1,2}, Phoebe A. Dunbar^{1,2}, Volker Wiebking³, Jesse D. Armitage^{4,5}, Isabelle Munoz^{1,2}, Kirsten L. Todd^{1,2}, Emily B. Derrick^{1,2}, Dat Nguyen^{1,2}, Junming Tong^{1,2}, Cheok Weng Chan^{1,2}, Thang X. Hoang^{1,2}, Katherine M. Audsley^{1,2}, Marit J. van Elsas^{1,2}, Jim Middelburg^{1,2}, Joel N. Lee^{1,2}, Maria N. de Menezes^{1,2}, Thomas J. Cole^{1,2}, Jasmine Li^{1,2}, Christina Scheffler^{1,2}, Andrew M. Scott^{6,7}, Laura K. Mackay⁸, Jason Waithman^{4,5}, Jane Oliaro^{1,2}, Simon J. Harrison^{2,9}, Ian A. Parish^{1,2}, Junyun Lai^{1,2}, Matthew H. Porteus³, Imran G. House^{1,2,12}, Phillip K. Darcy^{1,2,10,12} & Paul A. Beavis^{1,2,12} 

The efficacy of chimeric antigen receptor (CAR) T cell therapy in solid tumours is limited by immunosuppression and antigen heterogeneity^{1–3}. To overcome these barriers, ‘armoured’ CAR T cells, which secrete proinflammatory cytokines, have been developed⁴. However, their clinical application has been limited because of toxicity related to peripheral expression of the armouring transgene⁵. Here, we have developed a CRISPR knock-in strategy that leverages the regulatory mechanisms of endogenous genes to drive transgene expression in a tumour-localized manner. By screening endogenous genes with tumour-restricted expression, we have identified the *NR4A2* and *RGS16* promoters as promising candidates to support the delivery of cytokines such as IL-12 and IL-2 directly to the tumour site, leading to enhanced antitumour efficacy and long-term survival of mice in both syngeneic and xenogeneic models. This effect was concomitant with improved CAR T cell polyfunctionality, activation of endogenous antitumour immunity and a favourable safety profile, and was applicable in CAR T cells from patients.

Adoptive T cell therapy (ACT), including transgenic T cell receptor (TCR) therapy and CAR T cell therapy, has encouraging clinical potential for the treatment of cancer. In particular, CAR T cell therapy has achieved impressive outcomes in the treatment of haematological malignancies⁶. However, the lack of efficacy in the solid tumour setting continues to be a challenge, owing to a number of factors, including immunosuppression in the tumour microenvironment, tumour antigen heterogeneity and limited trafficking of CAR T cells to the tumour^{1–3}.

One promising approach to address these limitations is engineering T cells to express an immunomodulatory factor, such as a proinflammatory cytokine, that can enhance antitumour responses; these engineered cells are known as armoured T cells⁴. Several seminal studies have highlighted the potential of T cells armoured with cytokines such as interleukin-2 (IL-2)^{7,8}, IL-12 (refs. 9,10), IL-15 (ref. 11), IL-18 (refs. 12,13), Flt3L (ref. 14), interferon- γ (IFN γ)¹⁵ and IL-7/CCL19 (ref. 16). However, peripheral expression of proinflammatory cytokines can lead to toxicity, so this is a key concern when developing armoured T cells.

To address this, several strategies have been developed to restrict expression of the armouring transgene to the tumour site^{17–20}. Most of these rely on synthetic promoters and circuits to link transgene production to tumour-associated events such as TCR/CAR activation, including the nuclear factor of activated T cells (NFAT)-inducible promoter system¹⁷ and the synthetic Notch (SynNotch) system^{18,19}. However, when using these approaches, the control of gene expression is limited to short segments of regulatory DNA that are unable to fully encapsulate the nuances of gene regulation required for precise and site-specific gene expression. Indeed, both preclinical and clinical data indicate that the NFAT promoter system, which is currently the most widely used inducible system for armouring T cells, does not completely restrict transgene expression to the tumour site^{5,21,22}. This includes a clinical trial of NFAT-IL-12 armoured T cells that was prematurely terminated when severe toxicity occurred (NCT01236573)⁵. Thus, for armoured T cells to be a viable clinical option, more stringent regulatory mechanisms are required.

The advent of CRISPR introduced the ability to insert transgenes into specified genomic loci by homology-directed repair (HDR)^{23–25}.

¹Cancer Immunology Program, Peter MacCallum Cancer Centre, Melbourne, Victoria, Australia. ²Sir Peter MacCallum Department of Oncology, The University of Melbourne, Parkville, Victoria, Australia. ³Department of Pediatrics, Stanford University, Stanford, CA, USA. ⁴School of Biomedical Sciences, University of Western Australia, Perth, Western Australia, Australia. ⁵Leukaemia Translational Research Laboratory, Telethon Kids Cancer Centre, Telethon Kids Institute, Perth, Western Australia, Australia. ⁶Olivia Newton-John Cancer Research Institute and School of Cancer Medicine, La Trobe University, Melbourne, Victoria, Australia. ⁷Faculty of Medicine, The University of Melbourne, Parkville, Victoria, Australia. ⁸Department of Microbiology and Immunology at the Peter Doherty Institute for Infection and Immunity, The University of Melbourne, Parkville, Victoria, Australia. ⁹Clinical Haematology and Centre of Excellence for Cellular Immunotherapies, Peter MacCallum Cancer Centre and Royal Melbourne Hospital, Melbourne, Victoria, Australia. ¹⁰Department of Immunology, Monash University, Clayton, Australia. ¹¹These authors contributed equally: Amanda X. Y. Chen, Kah Min Yap. ¹²These authors jointly supervised this work: Imran G. House, Phillip K. Darcy, Paul A. Beavis.  e-mail: Amanda.chen@petermac.org; kahmin.yap@petermac.org; Phil.darcy@petermac.org; Paul.beavis@petermac.org

One application of this approach is to control transgene expression through the regulatory mechanisms of an endogenous gene. In this study, we proposed that we could leverage this ability to achieve tumour-localized expression of proinflammatory factors by CAR T cells and minimize systemic toxicity.

By screening for genes with increased transcriptional activity in intratumoral relative to splenic CAR T cells, we identified *NR4A2* and *RGS16* as promising promoters to support the tumour-directed delivery of proinflammatory factors. In particular, expressing transgenes through the *NR4A2* promoter led to superior tumour-restricted transgene expression when compared with a synthetic NFAT promoter-based approach. We further demonstrate that expression of IL-12 or IL-2 through the *NR4A2* or *RGS16* promoters, respectively, led to robust therapeutic responses without any overt signs of toxicity. By repurposing endogenous regulatory mechanisms to drive transgene expression, we propose that our approach will enable the development of next-generation armoured T cells with superior safety and efficacy compared with existing synthetic approaches.

Generation of CRISPR-edited armoured T cells

To develop and validate our CRISPR knock-in strategy, we selected *Pdcd1* as a prototype gene because its expression is increased in T cells on activation. We designed a homologous repair template to insert *GFP* immediately downstream of the *Pdcd1* start codon (Fig. 1a,b) and developed a protocol to achieve high-efficiency editing in primary murine T cells (Extended Data Fig. 1a–f). Notably, PD-1/GFP-edited OT-I cells significantly upregulated GFP expression after stimulation (Fig. 1c,d), indicating the successful control of GFP expression through the endogenous *Pdcd1* promoter.

Next, to assess whether the *Pdcd1* promoter drives transgene expression in a tumour-restricted manner *in vivo*, mock- or PD-1/GFP-edited OT-I cells were transferred to mice bearing AT-3 tumours expressing the ovalbumin antigen (AT-3-ova) (Fig. 1e,f). As expected, around 80% of mock OT-I cells expressed PD-1 in the tumour, with minimal PD-1 expression in the spleen. Indeed, in PD-1/GFP OT-I cells, this differential PD-1 expression was reflected through potent intratumoral GFP expression and significantly lower GFP expression in the spleen.

To assess the therapeutic potential and safety of HDR armoured T cells, we engineered OT-I cells to secrete proinflammatory cytokines that are toxic when administered systemically^{26,27}. TNF was selected for proof-of-concept experiments owing to its well-established role as a key effector cytokine and its ability to mediate bystander killing²⁸. PD-1/TNF-edited OT-I cells exhibited sustained TNF production after stimulation and enhanced bystander killing of antigen-negative tumour cells (Extended Data Fig. 2a–c).

In vivo, PD-1/TNF OT-I cells mediated significantly enhanced tumour control compared with mock and PD-1 knockout OT-I cells (Fig. 1g). Tumour-infiltrating PD-1/TNF OT-I cells exhibited enhanced TNF production and did not cause significant toxicity (Extended Data Fig. 2d,e). Similarly, PD-1/TNF CAR T cells demonstrated an increased capacity to produce TNF *in vitro* and enhanced antitumour efficacy *in vivo*, in a syngeneic hHer2 murine CAR T cell model (Extended Data Fig. 2f,g).

We next tested this system using other proinflammatory cytokines. Expression of IFNy, IL-2, IFN γ 9 or IFN β through the *Pdcd1* locus in OT-I cells led to significantly enhanced therapeutic responses without inducing overt toxicity (Fig. 1h). However, on assessment of PD-1/IL-12 OT-I cells, systemic toxicities characterized by rapid weight loss and significantly increased serum IL-12 levels were observed, so we euthanized the mice for ethical reasons (Fig. 1i–k). We proposed that these toxicities were attributed to unacceptably high levels of peripheral transgene expression when regulated by the *Pdcd1* promoter (Fig. 1f). We therefore sought to identify alternative promoters that may exhibit more favourable gene expression patterns than *Pdcd1*.

Identification of optimal target genes

To identify alternative target genes, we performed RNA-seq on CD8⁺ CAR T cells isolated from the tumour and spleen in both the syngeneic murine anti-hHer2 and xenogeneic human anti-Lewis Y (LeY) CAR T cell models (Extended Data Fig. 3a–i). Correlation of these datasets revealed many genes that were significantly upregulated by CAR T cells in the tumour relative to the spleen in both models (Fig. 2a), of which 27 were selected for further analysis based on the magnitude of differential expression (Supplementary Tables 1 and 2).

Of the 27 genes, 12 exhibited greater differential expression between the tumour and spleen compared with *PDCD1* in both CD8⁺ and CD4⁺ CAR T cells (red bars in Fig. 2b and Extended Data Fig. 3e–i). Next, each of the 27 genes was knocked out in human anti-LeY CAR T cells to evaluate the effects of gene disruption on cytokine production, cytotoxicity and proliferative capacity (Fig. 2c, Extended Data Fig. 4a–j and Supplementary Table 3). From these data, *AK4* and *FOSB* were excluded from further analyses because their disruption led to a marked reduction in cytokine production after CAR activation. Therefore, we proceeded to subsequent analyses with the top six genes identified on the basis of tumour specificity (*RGS16*, *CLU*, *RGS2*, *DUSP4*, *RGS1* and *NR4A2*) as well as *TNFAIP3*, owing to the enhanced cytokine production capacity observed after knockout.

Homologous repair templates were designed for HDR-mediated insertion of *GFP* into each of the seven shortlisted genes, with *PDCD1* included for comparison. *In vitro* stimulation of HDR-edited human anti-LeY CAR T cells with LeY-expressing tumour cells led to a significant induction in GFP expression in both CD8⁺ and CD4⁺ CAR T cells for four of the eight genes (*NR4A2*, *PDCD1*, *RGS16* and *RGS2*; Fig. 2d,e and Extended Data Fig. 5a–f). *DUSP4* and *TNFAIP3* exhibited high baseline GFP expression and were therefore excluded from subsequent analyses owing to their potential to cause toxicities.

We next assessed the ability of the remaining genes (*CLU*, *NR4A2*, *PDCD1*, *RGS1*, *RGS16* and *RGS2*) to drive tumour-restricted GFP expression in OVCAR-3 tumour-bearing mice (Fig. 2f–i). All promoters led to a significant increase in GFP expression in intratumoral relative to splenic CAR T cells (Fig. 2g,h). Notably, *CLU*/GFP, *NR4A2*/GFP and *RGS2*/GFP CAR T cells exhibited stringent tumour-restricted expression, with less than 10% of CAR T cells expressing GFP in the spleen. Of these three promoters, *NR4A2* supported the highest intratumoral GFP expression and was further verified to express minimal levels of GFP in the liver (Extended Data Fig. 5g,h), making it the top candidate for mediating safe payload delivery. By contrast, although *RGS16*/GFP CAR T cells demonstrated similar GFP expression levels in the spleen compared with PD-1/GFP CAR T cells, they expressed significantly higher GFP expression in the tumour (Fig. 2i). This indicated that the *RGS16* promoter may be ideal for transgenes that require potent intratumoral expression to mediate their antitumour effects. Thus, we identified two promising target genes for our CRISPR knock-in strategy to engineer armoured T cells (Fig. 2j), for which we could routinely obtain approximately 50% dual CAR and GFP expression after activation (Extended Data Fig. 5i).

NR4A2/IL-12 T cells are potent and safe

Given the tumour specificity of transgene expression when controlled by the *NR4A2* promoter, we proposed that this approach would support the safer delivery of IL-12. Consistent with our observations using the human *NR4A2* promoter, *NR4A2*/GFP OT-I cells exhibited significantly greater GFP expression following stimulation and, importantly, more tightly regulated GFP expression compared with PD-1/GFP OT-I cells (Fig. 3a and Extended Data Fig. 6a). Similarly, the *Nr4a2* promoter supported stringent tumour-restricted transgene expression *in vivo*, with less than 1% of OT-I cells expressing GFP in the spleen (Fig. 3b). This was in contrast to the significantly higher GFP expression observed in

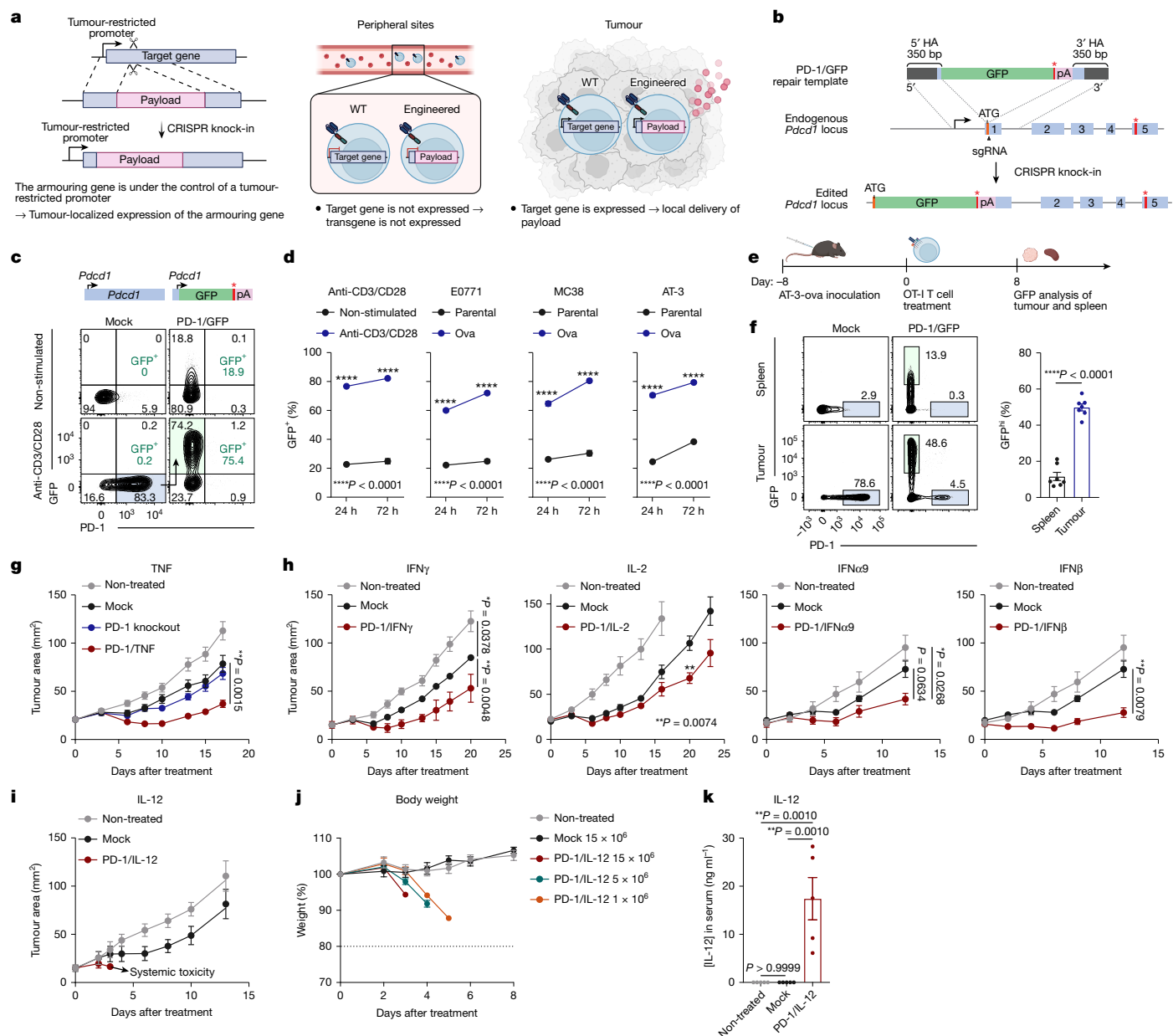


Fig. 1 | Development of a CRISPR knock-in strategy to engineer armoured T cells with tumour-restricted transgene expression. **a**, Schematic depicting the CRISPR knock-in approach. **b**, Design of the PD-1/GFP homologous repair template. **c,d**, Flow cytometry plots (c) and quantification of GFP expression (d) in mock or PD-1/GFP OT-I cells stimulated with anti-CD3/CD28 antibodies or the indicated tumour cell lines for 24 h or 72 h. Data are mean \pm s.d. of technical duplicates to triplicates, representative of $n = 3$ experiments. Red asterisks in **b,c** denote the location of a stop codon. **e,f**, Mock or PD-1/GFP OT-I cells were adoptively transferred into mice bearing AT-3-ova tumours and analysed 8 days after transfer. Experimental workflow (e) and data (f) showing flow cytometry plots (left) and quantification (right) of GFP expression in OT-I cells, shown as mean \pm s.e.m. from $n = 7$ mice per group. **g–k**, OT-I cells engineered to express the indicated cytokines through the *Pdcd1* locus were adoptively transferred

into mice bearing AT-3-ova tumours. Data are tumour growth curves (g–i); body weight of mice treated with the indicated doses (j); and serum IL-12 concentration (k) in mice treated with 5×10^6 OT-I cells at day 3 after treatment. Dashed line in j indicates 20% weight loss. Data in g–k are mean \pm s.e.m. from $n = 18$ mice per group pooled from $n = 3$ experiments (g) or $n = 6$ mice per group (IFN γ , IFN α 9 and IFN β), or $n = 4$ (non-treated, PD-1/IL-2) and 5 (mock) mice per group (IL-2), representative of $n = 2$ (IFN α 9 and IFN β) or 3 (IFN γ and IL-2) experiments (h); $n = 5$ mice per group (i–k). **d,g**, Two-way analysis of variance (ANOVA); **f**, two-sided paired *t*-test; **h**, two-way ANOVA (IFN γ , IFN α 9 and IFN β) and two-sided unpaired *t*-test (IL-2); **k**, one-way ANOVA. $^*P < 0.05$, $^{**}P < 0.01$, $^{***}P < 0.0001$. Illustrations in a and e created using BioRender: a, Chen, A., <https://Biorender.com/y6lxgqk> (2025); e, Chen, A., <https://Biorender.com/dzaw25> (2025).

splenic PD-1/GFP OT-I cells, which likely explains the toxicities elicited by PD-1/IL-12 OT-I cells (Fig. 1i–k).

Based on the above findings, we assessed the therapeutic efficacy and safety of NR4A2/IL-12 OT-I cells after confirming successful *IL-12* integration (Extended Data Fig. 6b). Strikingly, NR4A2/IL-12 OT-I cells demonstrated significantly enhanced efficacy (Fig. 3c,d), an effect that was maintained even with a lower dose of 1×10^6 T cells (Extended Data

Fig. 6c,d). Importantly, in contrast to PD-1/IL-12 OT-I cells, no toxicity was observed in mice treated with NR4A2/IL-12 OT-I cells (Fig. 3e).

Similarly, NR4A2/GFP CAR T cells exhibited superior tumour-restricted transgene expression compared with PD-1/GFP CAR T cells (Extended Data Fig. 6e,f). We further compared this approach with the NFAT promoter system (Fig. 3f), which is regarded as the gold standard for engineering tumour-inducible armoured T cells.

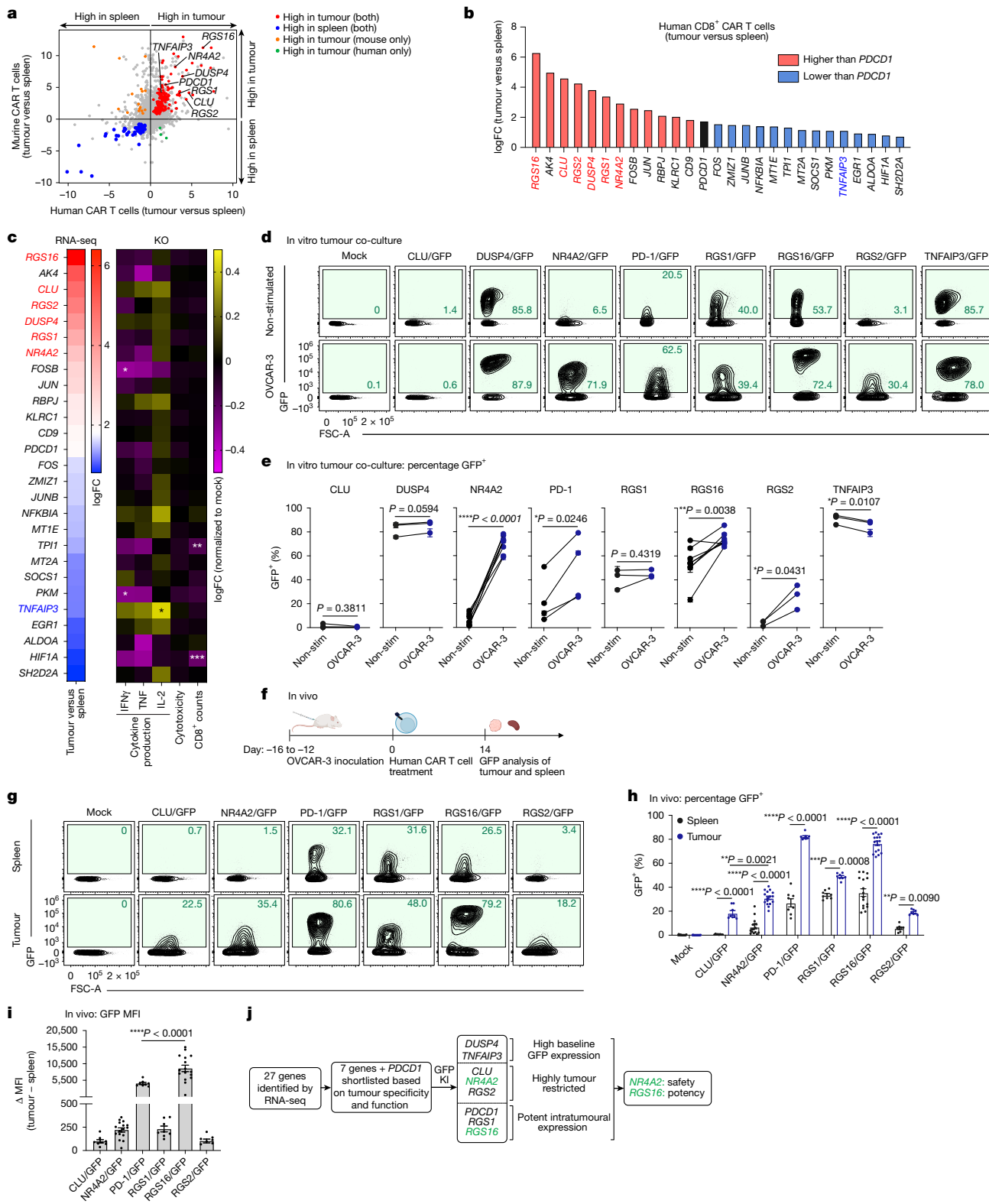


Fig. 2 | See next page for caption.

As expected, NFAT–GFP anti-hHer2 CAR T cells expressed limited GFP before activation (Fig. 3g). However, in vivo, NFAT–GFP CAR T cells exhibited significant GFP expression (about 10%) in the spleen, blood, liver, lung, brain, kidney and bone marrow, whereas NR4A2/GFP CAR T cells retained a maximum of 2% GFP expression in all the peripheral sites tested (Fig. 3h,i). The systemic GFP expression by NFAT–GFP CAR

T cells was sustained over time, and we observed this in both parental (hHer2-negative) tumour- and non-tumour-bearing mice, and it was recapitulated using human CAR T cells (Extended Data Fig. 6g–j). Taken together, these data reveal that the endogenous *Nr4a2* promoter supports more stringent tumour-restricted transgene expression than the synthetic NFAT promoter.

Fig. 2 | Identification of optimal target genes for CRISPR-engineered armoured T cells. **a, b**, Bulk RNA sequencing of CD8⁺ murine anti-hHer2 or human anti-LeY CAR T cells from tumours and spleens of E0771-hHer2 or OVCAR-3 tumour-bearing mice at day 8 or 9 after treatment, respectively. Correlation plot of murine and human CAR T cell data (**a**) and log fold change (logFC) in expression of top 27 genes with high differential expression between intratumoral and splenic human CAR T cells (**b**); red, higher logFC than *PDCD1*; blue, lower logFC than *PDCD1*. Data are representative of $n = 2$ biological replicates. **c**, Heatmaps showing logFC in expression (tumour versus spleen) for the 27 genes shown in **b** (left), and the impact of their CRISPR/Cas9-mediated knockout (KO) on the proliferation of human anti-LeY CAR T cells and their cytokine-producing and killing capacities following OVCAR-3 tumour cell co-culture (right). Knockout data represent logFC normalized to mock CAR T cells pooled from $n = 3$ donors. Coloured text highlights genes that were selected for further analysis via CRISPR-mediated *GFP* knock-in. **d, e**, Human

anti-LeY CAR T cells engineered to express GFP were co-cultured with OVCAR-3 tumour cells for 72 h. Flow cytometry plots (**d**) and quantification (**e**) of GFP expression in CD8⁺ CAR T cells, represented as mean \pm s.d. of technical triplicates from $n = 3$ (CLU, DUSP4, RGS1, RGS2 and TNFAIP3), 4 (PD-1) or 8 (NR4A2 and RGS16) donors. FSC-A, forward scatter area. **f–i**, Human anti-LeY CAR T cells adoptively transferred into mice bearing OVCAR-3 tumours were assessed 14 days after transfer. MFI, mean fluorescence intensity. Data are experimental workflow (**f**); flow cytometry plots (**g**); quantification of GFP percentage (**h**) and Δ MFI (**i**) in intratumoral and splenic CD8⁺ CAR T cells, showing mean \pm s.e.m. from $n = 8$ mice per group pooled from $n = 2$ donors (CLU, PD-1, RGS1 and RGS2) and $n = 16$ mice per group pooled from $n = 4$ donors (NR4A2 and RGS16). **j**, Flow chart summarizing the identification of *NR4A2* and *RGS16* (green text). **c, i**, One-way ANOVA; **e**, two-sided paired *t*-test; **h**, two-way ANOVA. * $P < 0.05$, ** $P < 0.01$, *** $P < 0.001$, **** $P < 0.0001$. Illustrations in **f** created using BioRender: Chen, A., <https://BioRender.com/dzaw25> (2025).

Murine CAR T cells were then engineered to express IL-12 through the *Nr4a2* promoter (Extended Data Fig. 6k) and assessed for therapeutic efficacy against E0771-hHer2 and MC38-hHer2 tumours, the latter of which we have previously shown to be refractory to anti-hHer2 CAR T cell treatment^{29,30}. NR4A2/IL-12 murine CAR T cells demonstrated a significantly enhanced therapeutic effect and increase in mouse survival, even against larger, more advanced tumours in the absence of toxicities (Fig. 3j,k and Extended Data Fig. 6l,m). By contrast, severe toxicities were observed with NFAT-IL-12 murine CAR T cells in E0771-hHer2 tumour-bearing mice, as indicated by their rapid weight loss (Extended Data Fig. 6n,o), hunching and inactivity (Supplementary Information 1–4). Together, these data demonstrate the ability of the *Nr4a2* promoter to drive highly tumour-localized transgene expression without eliciting systemic toxicities.

Activation of host antitumour immunity

We next sought to assess the mechanism by which NR4A2/IL-12 T cells elicit enhanced therapeutic activity. In the OT-I model, intratumoral NR4A2/IL-12 OT-I cells exhibited an increased capacity to secrete IFN γ and TNF following ex vivo stimulation with the SIINFEKL peptide, as well as significantly elevated Ki67 expression (Fig. 4a–c), although no differences in T cell numbers were observed at the assessed time point (Extended Data Fig. 7a). Consistent with their more activated phenotype, splenic NR4A2/IL-12 OT-I cells exhibited a marked increase in the proportion of the CD62L[−]CD44⁺ effector memory-like subset, as well as PD-1 and Tim3 expression (Fig. 4d and Extended Data Fig. 7b,c).

Previous studies have demonstrated the importance of epitope spreading in mediating a robust therapeutic response after ACT^{14,31}. Using congenic CD45.1⁺ recipient mice, we observed that mice treated with NR4A2/IL-12 OT-I (CD45.2⁺) cells had an increased frequency of ova-specific host (CD45.1⁺) CD8⁺ T cells in the spleen (Fig. 4e). Furthermore, ex vivo stimulation of tumours and tumour-draining lymph nodes (dLNs) with the SIINFEKL peptide revealed a significantly increased number of IFN γ - and TNF-producing endogenous CD8⁺ T cells, which was concomitant with an increased number of Ki67⁺ host CD8⁺ T cells in the tumour (Fig. 4f and Extended Data Fig. 7d,e).

Similarly, we observed significantly increased numbers of CD8⁺ T cells in MC38-hHer2 tumours treated with NR4A2/IL-12 murine anti-hHer2 CAR T cells, concomitant with significantly increased Ki67 expression (Fig. 4g–i). Using a tetramer specific to the p15E antigen, which is expressed on MC38 tumour cells³², we observed a significant increase in the frequency of tumour-specific CD8⁺ T cells in the spleens of mice treated with NR4A2/IL-12 CAR T cells (Fig. 4j). This was supported by an increased number of IFN γ - and TNF-producing CD8⁺ T cells following ex vivo stimulation of tumours with a cocktail of defined MC38 neoantigen peptides (Fig. 4k). To further investigate the epitope spreading mediated by NR4A2/IL-12 CAR T cells, we performed bulk

TCR sequencing on the tumour dLN of a mouse that exhibited a high frequency of tumour-specific endogenous CD8⁺ T cells in the spleen and tumour (data point 1 in Fig. 4j,k). This revealed an oligoclonal expansion of several TCR clonotypes, indicating the stimulation of an endogenous T cell response beyond the p15E antigen (Fig. 4l). This was also observed following subsequent TCR sequencing of tumour dLN samples from a further three mice (data points 2, 3 and 4 in Fig. 4j,k) that exhibited an intermediate frequency of p15E-specific T cells (Fig. 4m). Furthermore, tumour rechallenge experiments revealed that mice previously cured by NR4A2/IL-12 CAR T cells exhibited significant protection against parental E0771 or MC38 tumours relative to treatment-naive mice (Extended Data Fig. 7f,g), providing further evidence of epitope spreading against non-hHer2 antigens.

Efficacy of human armoured CAR T cells

To extend these findings into a human tumour model, we first engineered NR4A2/IL-12 human anti-LeY CAR T cells, which expanded equivalently to control CAR T cells and produced increased levels of not only IL-12, but also IFN γ , TNF and IL-2 following in vitro stimulation (Extended Data Fig. 8a–c). In vivo, NR4A2/IL-12 CAR T cells mediated significantly enhanced antitumour responses against OVCAR-3 tumours relative to mock-edited CAR T cells, and cured mice showed increased resistance against a secondary challenge with OVCAR-3 tumours (Fig. 5a,b and Extended Data Fig. 8d,e). Notably, this occurred without observable toxicities, in contrast to PD-1/IL-12 CAR T cells, which induced rapid weight loss (Extended Data Fig. 8f).

We found that NR4A2/IL-12 CAR T cells had significantly enhanced expression of IFN γ , TNF, granzyme B (GzmB) and Ki67 (Fig. 5c–e and Extended Data Fig. 8g–i), and both CD8⁺ and CD4⁺ CAR T cells were present at higher frequencies in the tumour, spleen and blood (Extended Data Fig. 8j,k). RNA-seq of intratumoral CD8⁺ CAR T cells revealed significant differences between NR4A2/IL-12 and mock-edited CAR T cells including, unsurprisingly, increased expression of genes associated with IL-12 signalling, such as *IFNG* and *IL18R1* (Fig. 5f and Extended Data Fig. 9a). Gene set enrichment analysis (GSEA) revealed significant upregulation of genes associated with proliferation, TNF signalling and STAT3/4/5 signalling, highlighting the increased effector functionality of NR4A2/IL-12 CAR T cells (Fig. 5g and Extended Data Fig. 9b,c).

To further explore the applicability of the *NR4A2* promoter, we engineered human anti-LeY CAR T cells to express IL-2 (Extended Data Fig. 10a). However, NR4A2/IL-2 CAR T cells mediated only a mild enhancement of tumour control in vivo (Fig. 5h). We thus proposed that the *RGS16* promoter may be more suited to the delivery of IL-2, given its ability to support greater intratumoral transgene expression (Fig. 2g–j). Indeed, RGS16/IL-2 CAR T cells exhibited significantly higher IL-2 expression (Extended Data Fig. 10a,b) and a superior antitumour

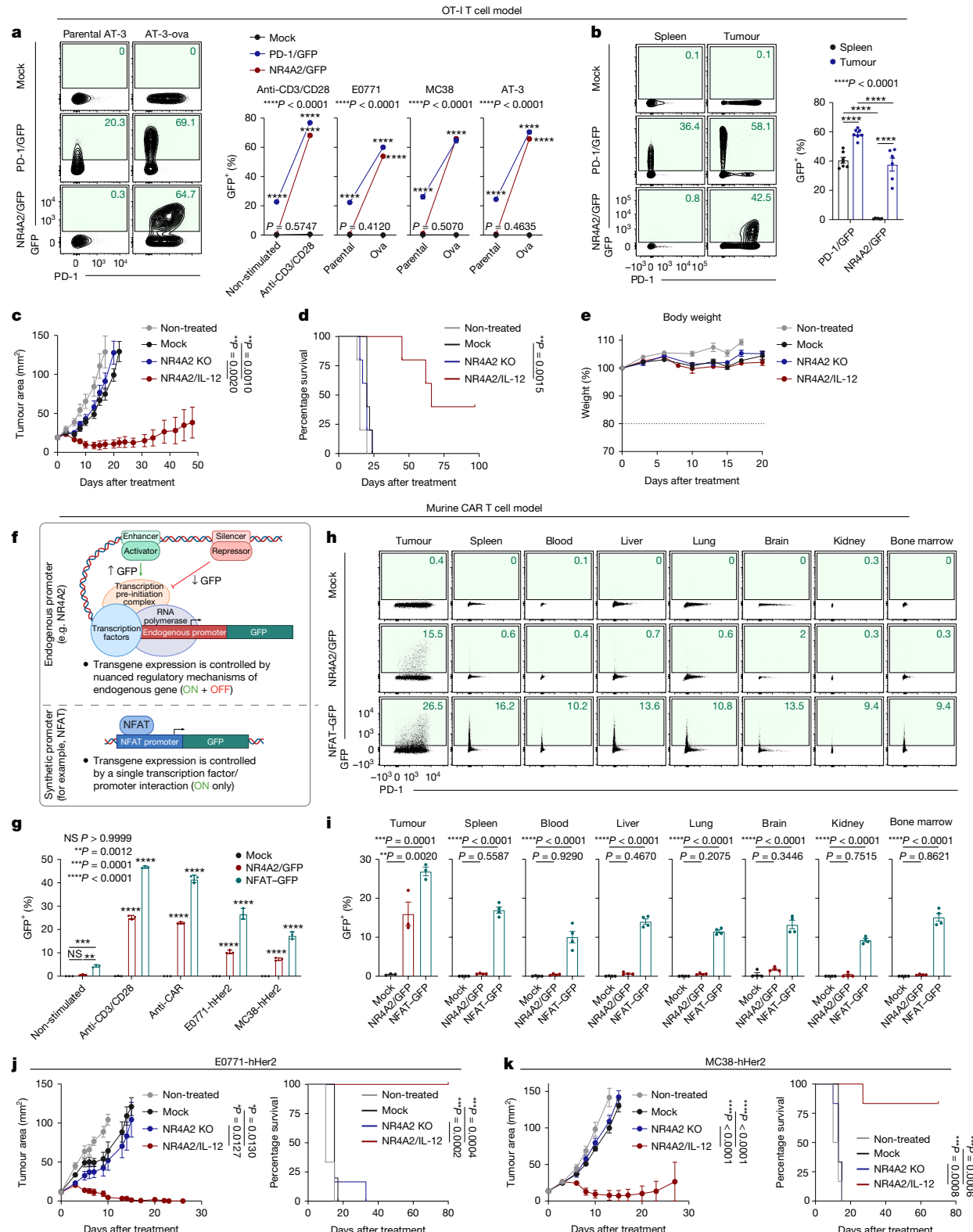


Fig. 3 | See next page for caption.

effect compared with NR4A2/IL-2 and PD-1/IL-2 CAR T cells (Fig. 5h). Importantly, toxicity was not observed (Extended Data Fig. 10c), indicating that the *RGS16* promoter is suitable for driving intratumoral expression of factors with a milder toxicity profile. Mechanistically, RGS16/IL-2 CAR T cells exhibited significantly increased Ki67, IFN γ and TNF expression and significantly greater numbers of both CD8⁺

and CD4⁺ CAR T cells in the tumour, spleen and blood (Fig. 5i–k and Extended Data Fig. 10d,e). Moreover, in an immunocompetent setting, RGS16/IL-2 murine anti-hHer2 CAR T cells mediated significantly enhanced therapeutic efficacy against E0771-hHer2 tumours and, importantly, did not lead to a significant increase in intratumoral T_{reg} cells (Extended Data Fig. 10f,g).

Fig. 3 | NR4A2/IL-12 engineered T cells are well tolerated and elicit potent antitumour immunity. **a,b**, OT-I cells engineered to express GFP were assessed after 24-hour stimulation with anti-CD3/CD28 antibodies or ova-expressing tumour cells (**a**) and in mice bearing AT-3-ova tumours 8 days after transfer (**b**). Flow cytometry plots (left) and quantification (right) of GFP expression in OT-I cells. **c–e**, We adoptively transferred 12.5×10^6 mock, NR4A2 knockout or NR4A2/IL-12 OT-I cells into mice with AT-3-ova tumours. Data are tumour growth (**c**), survival (**d**) and body weight (**e**). **f**, Schematic depicting differences between endogenous and synthetic promoters. **g–i**, Murine anti-Her2 CAR T cells expressing GFP through synthetic NFAT or endogenous *Nr4a2* promoters were assessed after 24-hour stimulation with anti-CD3/CD28, anti-CAR antibodies or hHer2-expressing tumour cells (**g**) and in E0771-hHer2 tumour-bearing mice 9 days after transfer (**h,i**). Flow cytometry plots (**h**) and quantification (**g and i**) of GFP expression in CD8⁺ CAR T cells. **j,k**, 5×10^6 mock,

NR4A2 knockout or NR4A2/IL-12 murine anti-hHer2 CAR T cells were adoptively transferred into E0771-hHer2 (**j**) or MC38-hHer2 (**k**) tumour-bearing mice. Data are tumour growth (left) and survival (right). **a,g**, Data are mean \pm s.d. of technical triplicates, representative of $n = 3$ (**a**) and $n = 2$ (**g**) experiments. **b–e,h–k**, Data are mean \pm s.e.m. from $n = 6$ (NR4A2/GFP) or 7 (PD-1/GFP) mice per group, representative of $n = 3$ experiments (**b**); $n = 5$ mice per group (**c–e**); $n = 3$ (tumour) and 4 (non-tumour tissues) mice per group (**h,i**); $n = 4$ (NR4A2/IL-12), $n = 5$ (mock) and $n = 6$ (non-treated, NR4A2 knockout) mice per group (left), or $n = 5$ (mock), $n = 6$ (non-treated, NR4A2 knockout) and $n = 7$ (NR4A2/IL-12) mice per group (right), representative of $n = 2$ experiments (**j**); $n = 6$ mice per group (**k**). **a–c,g,j–k** (Left), two-way ANOVA; **d,j–k** (right), log-rank Mantel-Cox test; **i**, one-way ANOVA. NS, not significant; $^*P < 0.05$, $^{**}P < 0.01$, $^{***}P < 0.001$, $^{****}P < 0.0001$. Illustrations in **f** created using BioRender: Chen, A., <https://BioRender.com/03b4c93> (2025).

Clinical applicability of knock-in approach

Finally, we assessed the applicability of this technology to the patient setting. To interrogate the transcriptional activity of the *NR4A2* and *RGS16* promoters in patient T cells, we analysed publicly available scRNA-seq data for their expression in T cells from the blood and tumour across a broad range of cancer types³³. This revealed a higher frequency of both *NR4A2*- and *RGS16*-expressing T cells in the tumour than in peripheral blood (Fig. 5*l*), indicating that these genes are likely to support tumour-localized transgene expression across diverse tumour types when engineered through our CRISPR knock-in approach.

We also investigated whether patient-derived T cells could be reprogrammed by our CRISPR knock-in strategy. Anti-LeY CAR T cells derived from patients with diffuse large B cell lymphoma (DLBCL) or multiple myeloma had similar results to healthy donor CAR T cells, with stringent CAR-inducible GFP expression in NR4A2/GFP CAR T cells and potent GFP expression in RGS16/GFP CAR T cells (Fig. 5*m–o* and Extended Data Fig. 11*a–c*). Furthermore, NR4A2/IL-12 and RGS16/IL-2 patient CAR T cells had the expected cytokine profiles following stimulation *in vitro* (Fig. 5*p* and Extended Data Fig. 11*d*).

We then assessed the sensitivity of our system against varying antigen densities, to more closely mimic the clinical setting. In the murine system, NR4A2/GFP and RGS16/GFP anti-hHer2 CAR T cells exhibited a similar capacity to upregulate GFP expression against MC38 tumours with low versus high hHer2 expression (Extended Data Fig. 11*e,f*). In the human system, stimulation of NR4A2/GFP and RGS16/GFP anti-LeY CAR T cells with suboptimal concentrations of anti-LeY idiotypic antibodies resulted in significant GFP upregulation (Extended Data Fig. 11*g,h*). Furthermore, NR4A2/GFP human anti-hHer2 CAR T cells exhibited stringent GFP expression against MDA-MB-231 tumour cells, which have low hHer2 expression (Extended Data Fig. 11*i,j*). We also demonstrated that our system is sensitive in contexts of suboptimal antigen recognition, because NR4A2/IL-12 and RGS16/IL-2 OT-3 cells, which have low avidity for the ovalbumin antigen, exhibited substantial IL-12 and IL-2 expression, respectively, following stimulation with AT-3-ova tumour cells (Extended Data Fig. 11*k*). Together, these data demonstrate the ability of the *NR4A2* and *RGS16* promoters to support transgene expression against low antigen densities and TCR affinities.

Previous studies have demonstrated the merits of CAR expression through the *TRAC* locus²³. We therefore explored the use of a one-step manufacturing protocol to simultaneously knock-in a transgene into *NR4A2* or *RGS16* and a CAR into the *TRAC* locus. Comparison of human anti-LeY CAR T cells generated using our original two-step protocol with those from the one-step protocol revealed similar CAR expression, transgene knock-in efficiencies and *in vivo* efficacy (Fig. 5*q–s* and Extended Data Fig. 12*a–d*). Together, these data demonstrate the clinical potential of our CRISPR knock-in approach to engineer armoured CAR T cells, in which the endogenous regulatory machinery of tumour-restricted genes, including *NR4A2* and *RGS16*, are leveraged to drive localized expression of proinflammatory cytokines.

Discussion

Engineering T cells to express a proinflammatory factor is a promising strategy to elicit a robust, multifaceted therapeutic response in the treatment of solid tumours, but it has the potential to cause toxicities, owing to peripheral transgene expression. In this study, we present a new CRISPR knock-in approach that leverages endogenous gene regulatory mechanisms to express transgenes in a tumour-localized manner.

The use of endogenous tumour-restricted promoters to drive transgene expression provides enhanced regulatory control compared with synthetic promoter systems. First, coupling transgene expression to an endogenous gene enables its control by not only the promoter but all *trans*- and *cis*-regulatory elements of the endogenous gene, the latter of which can extend up to 1 megabase from the gene locus^{34,35}. By contrast, synthetic promoters use only a short segment of regulatory DNA and rely on simple promoter/transcription factor interactions to initiate gene expression. This provides 'on' signals but lacks mechanisms to fine-tune or switch off gene expression when required. This may explain the inability of the NFAT promoter to restrict transgene expression to the tumour *in vivo*, as observed in our study, as well as other reports of its leaky transgene expression^{13,21,22} and potential to cause systemic toxicities^{5,20}. Although more-recent inducible systems have been proposed, including variations of the NFAT system³⁶, alternative T cell activation-dependent promoters³⁷, logic-gating strategies, such as the SynNotch system¹⁸, and drug-inducible or physically induced systems²⁰, these also rely on synthetic regulatory elements and so may encounter similar limitations to the NFAT system.

Our CRISPR knock-in strategy also offers greater flexibility over T cell design. Although the *NR4A2* promoter is ideal for expressing highly toxic factors such as IL-12, the *RGS16* promoter enables potent intratumoral transgene expression and may be more favourable for delivering less-toxic factors, such as IL-2. Thus, promoter choice can be tailored to the specific transgene of interest. Moreover, our study used a 'knock-in, knock-out' approach in which target gene expression is disrupted following transgene integration, potentially enabling further enhancement of T cell function by target gene knockout. Functionally, *NR4A2* and *RGS16* have been demonstrated to promote T cell exhaustion and limit antitumour T cell responses^{38–40}, with one study observing enhanced therapeutic efficacy in NR4A2-knockout CAR T cells³⁸. Although *NR4A2* and *RGS16* depletion was not observed to enhance CAR T cell function in our studies, this does not rule out the possibility that their depletion may be beneficial in a clinical context.

Our mechanistic studies of NR4A2/IL-12-engineered T cells complement and extend previous findings on the antitumour functions of IL-12 (refs. 9,10). NR4A2/IL-12 OT-I and CAR T cells not only exhibited an enhanced proinflammatory phenotype, but also demonstrated an ability to engage host antitumour immunity, leading to the emergence of CD8⁺ T cells that recognize antigens not targeted by the OT-ITCR or CAR. Given the heterogeneity of antigen expression in solid tumours,

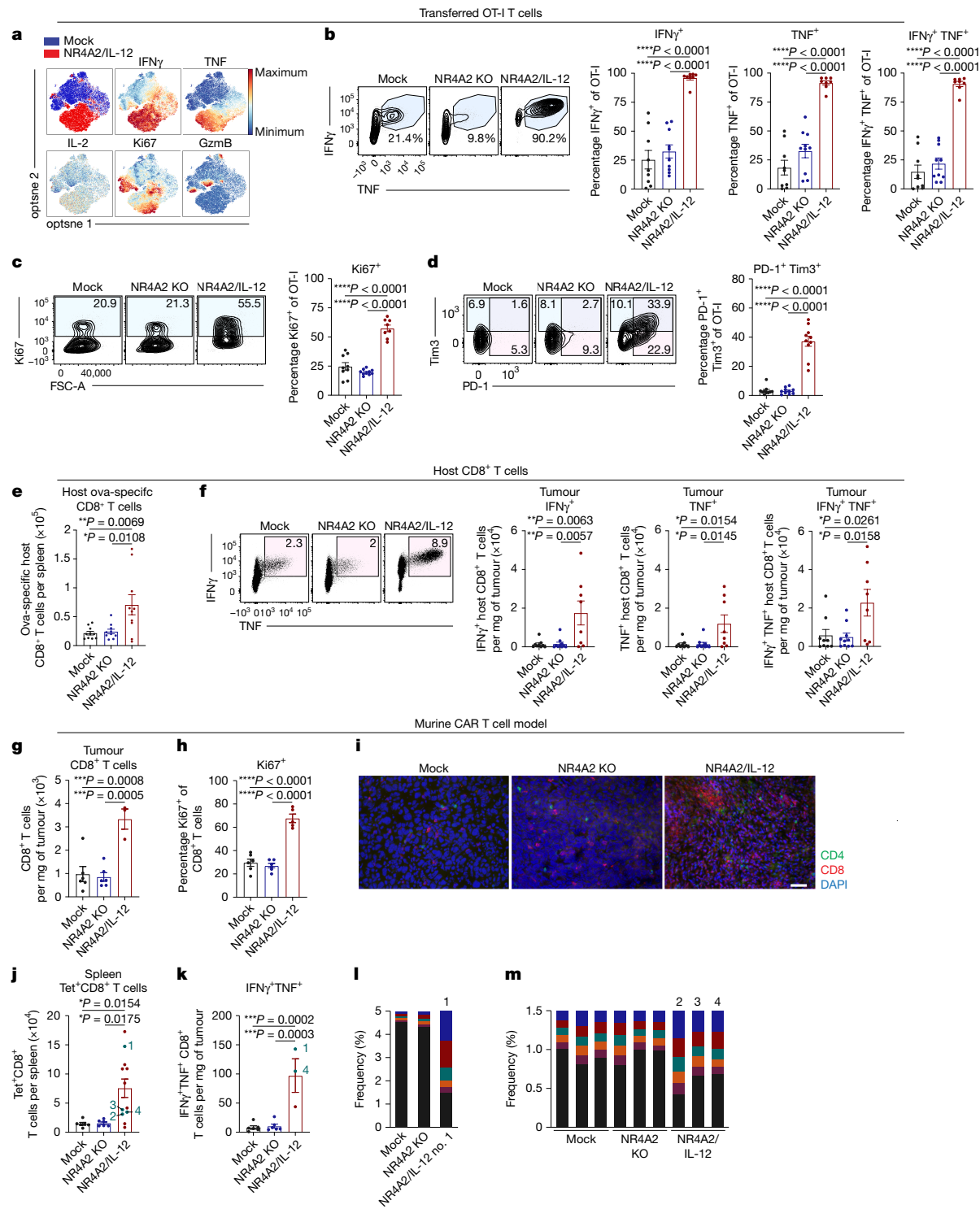


Fig. 4 | NR4A2/IL-12 engineered T cells exhibit an enhanced proinflammatory phenotype and effectively promote host antitumour immunity. **a–f**, Mock, NR4A2 knockout or NR4A2/IL-12 OT-I cells (CD45.2⁺) were adoptively transferred into CD45.1⁺ mice bearing AT-3 ova tumours, and ex vivo analyses were performed 8 days later. Data are t-SNE plots comparing protein expression in intratumoral OT-I cells (**a**); flow cytometry plots (left) and quantification (right) of IFN γ , TNF, Ki67, PD-1 and Tim3 expression in intratumoral (**b**, **c**) or splenic (**d**) OT-I cells; quantification of H-2K b SIINFEKL tetramer⁺ host splenic CD8⁺ T cells (**e**); and flow cytometry plots (left) and quantification (right) of IFN γ and TNF expression in host intratumoral CD8⁺ T cells (**f**). **g–m**, 5×10^6 mock, NR4A2 knockout or NR4A2/IL-12 murine anti-hHer2 CAR T cells were adoptively transferred into MC38-hHer2 tumour-bearing mice and ex vivo analyses were performed 9 days later. Data are quantification of intratumoral CD8⁺ T cells (**g**)

and their Ki67 expression (**h**); immunofluorescence imaging of tumours showing CD4, CD8 and DAPI, representative of $n = 3$ mice per group (**i**); quantification of H-2K b p15E tetramer⁺ splenic CD8⁺ T cells (**j**) and IFN γ ⁺ TNF⁺ intratumoral CD8⁺ T cells (**k**); green data points indicate mice with tumour dLNs analysed by TCR sequencing (**l**–**m**), showing cumulative frequencies of the top five TCR clonotypes (indicated by five colours; black indicates all other TCR clonotypes) in tumour dLNs. **a–c, f, k**, Tumours were ex vivo stimulated with SIINFEKL (**a–c, f**) or MC38 neoantigen peptides (**k**) for 3 h. **a–d, f**, Plots concatenated from $n = 5$ mice per group. **b–h, j–k**, Data are mean \pm s.e.m. from $n = 8$ (NR4A2/IL-12), $n = 9$ (mock) and $n = 10$ (NR4A2 knockout) mice per group (**b–h**) or $n = 10$ mice per group (**d, e**) pooled from $n = 2$ experiments; $n = 6$ (mock, NR4A2 knockout) and $n = 3$ (**g, k**) or $n = 5$ (**h**) or $n = 12$ (**j**) (NR4A2/IL-12) mice per group. One-way ANOVA. * $P < 0.05$, ** $P < 0.01$, *** $P < 0.001$, **** $P < 0.0001$. Scale bar in **i**, 50 μ m.

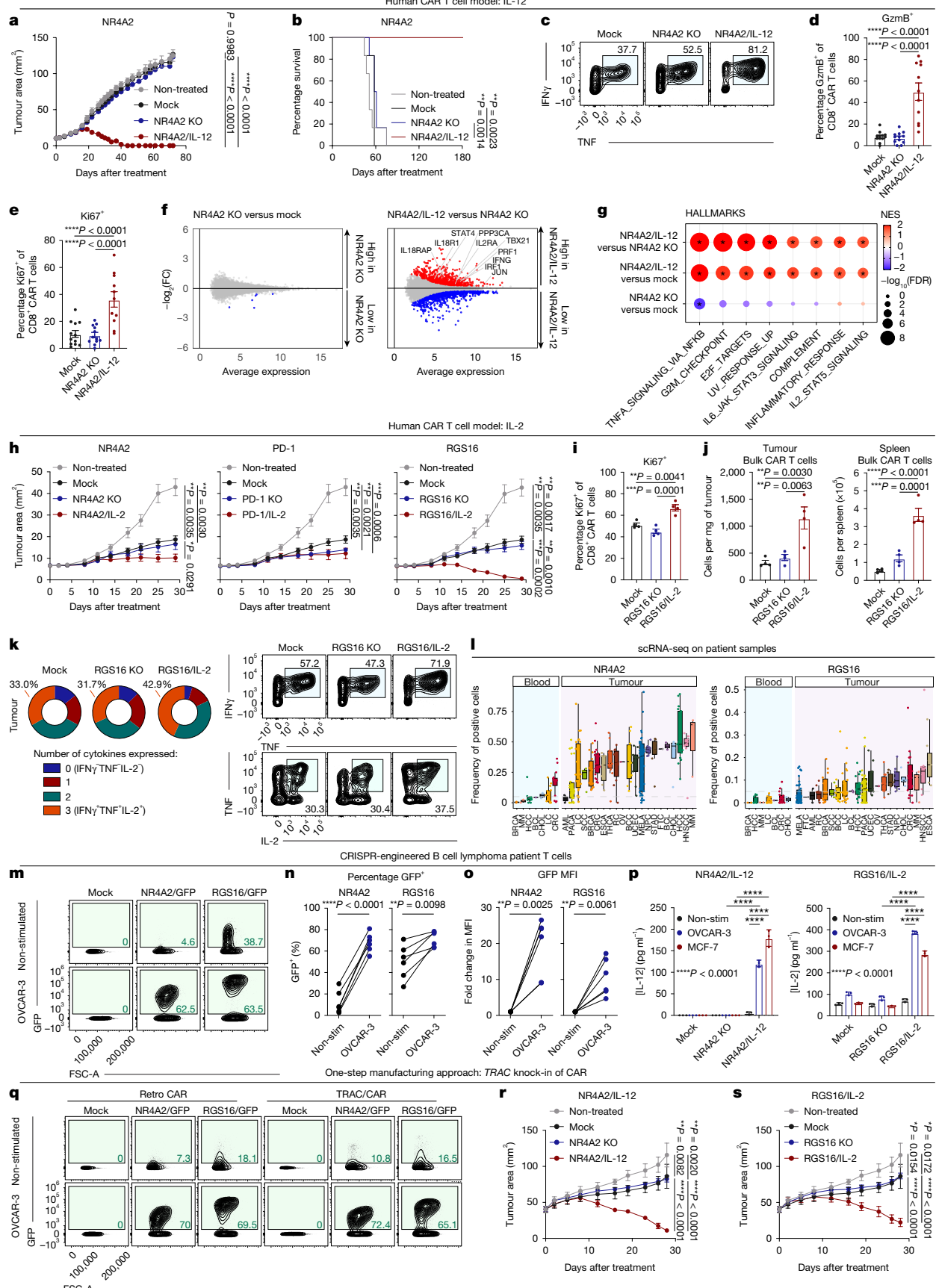


Fig. 5 | See next page for caption.

Fig. 5 | Therapeutic efficacy and clinical applicability of CRISPR-engineered human CART cells. **a–k**, Human anti-LeY CART cells engineered to express IL-12 (a–g) or IL-2 (h–k) were transferred into OVCAR-3 tumour-bearing mice, with CD8⁺ (c–g,i,k) or bulk (j) CART cells analysed ex vivo 11–14 days later. Data are tumour growth (a,h); survival (b); intratumoral IFN γ and TNF expression (c); peripheral blood GzmB (d) and Ki67 expression (e); transcriptomic comparison of indicated intratumoral CART cells (f); GSEA of indicated pathways (false discovery rate (FDR) < 0.05) (g); intratumoral Ki67 expression (i); frequencies of intratumoral and splenic CART cells (j); and proportion of cytokine-expressing intratumoral CART cells (k). Tumours were PMA/ionomycin-restimulated for 3 h (c,i,k). NES, normalized enrichment score. **l**, Frequencies of patient T cells expressing *NR4A2* or *RGS16* were reanalysed from ref. 33 (TCGA abbreviations). Boxes represent the interquartile range (IQR), with whiskers extended to the maximum and minimum values within 1.5 IQR. Lines within boxes denote the median value. **m–p**, DLBCL patient-derived anti-LeY CART cells were CRISPR-engineered and stimulated in vitro. Data show GFP expression in CD8⁺ CAR

T cells after 72 h (m–o) and IL-12/IL-2 concentrations after 24 h (p). **q–s**, Anti-LeY CART cells generated by retroviral transduction or *TRAC*-targeted knock-in, with simultaneous GFP/IL-12/IL-2 knock-in to *NR4A2/RGS16*, were assessed in vitro (q) and in OVCAR-3 tumour-bearing mice (r,s). Data are GFP expression in CD8⁺ CART cells after 24 h (q) and tumour growth (r,s). **a–e,h–k,r,s**, Data are mean \pm s.e.m. from $n = 5$ (NR4A2/IL-12) and $n = 6$ (non-treated, mock and NR4A2 knockout) mice per group (a,b); $n = 4$ mice per group (c,i–k,r,s); $n = 11$ (NR4A2/IL-12) and $n = 12$ (mock and NR4A2 knockout) mice per group pooled from $n = 2$ experiments (d,e); $n = 3$ (NR4A2 knockout), $n = 5$ (PD-1 knockout and RGS16/IL-2) and $n = 6$ (non-treated, mock, NR4A2/IL-2, PD-1/IL-2 and RGS16 knockout) mice per group (h). **f,g**, Data from $n = 2$ biological replicates of $n = 8$ mice per group. **m–q**, Data represent mean \pm s.d. of technical triplicates, from $n = 6$ donors (m–o). **a,h,p,r,s**, Two-way ANOVA; **b**, log-rank Mantel–Cox test; **d,e,i–j**, one-way ANOVA; **n,o**, two-sided paired *t*-test. * $P < 0.05$, ** $P < 0.01$, *** $P < 0.001$, **** $P < 0.0001$.

this ability of IL-12 to mediate epitope spreading would synergize with and broaden the therapeutic potential of ACT, which often targets only a single antigen. We further observed that NR4A2/IL-12 CART cells mediated increased CD8⁺ T cell numbers in MC38-hHer2 tumours, which are generally poorly infiltrated by standard CART cells^{29,30}. This highlights the ability of our approach to overcome the challenge posed by limited trafficking of CART cells to solid tumours.

Furthermore, our CRISPR knock-in approach has the potential for clinical translation, demonstrated by our successful engineering of DLBCL and multiple myeloma patient T cells. Moreover, the ability to simultaneously insert a transgene into *NR4A2* or *RGS16* and a CAR into the *TRAC* locus through a ‘one-step’ approach would streamline the clinical production of CRISPR-engineered armoured CART cells. The feasibility of this approach is supported by ongoing clinical trials (NCT04438083, NCT04502446 and NCT04244656) assessing CART cells with CAR knock-in to the *TRAC* locus and simultaneous disruption of genes such as those encoding MHC-I and TCR β . However, a key consideration of CRISPR engineering is the potential for detrimental off-target effects. Indeed, a low frequency of off-target indels have been detected in CRISPR-engineered T cells, although no phenotypic abnormalities or post-treatment toxicities were observed following infusion into patients^{41,42}. Furthermore, simultaneously targeting multiple loci may lead to large chromosomal aberrations⁴²; however, these were observed at a low frequency that decreased to undetectable levels following adoptive transfer.

One limitation of our approach is that although it achieves improved tumour-restricted expression compared to the NFAT system, the risk of on-target, off-tumour toxicity remains. Therefore, the choice of target antigen will be extremely important. In this regard, LeY, as used in our study, is an attractive target, given its lack of expression in healthy tissues^{43,44}, as well as clinical data highlighting the safety of anti-LeY CART cells⁴⁵ (NCT03851146). Recent clinical data with CARs targeting STEAP2 and GPC3 indicate that these are also promising targets, owing to their low expression in healthy tissues^{46–48}. Alternatively, our approach could be used in neoantigen-specific T cells, because neoantigens are absent in healthy tissues.

Broadly, our CRISPR knock-in approach can be used to express almost any DNA-encoded factor in a tumour-restricted manner, enabling future studies to explore different applications of our system⁴⁹. For example, the increased frequency of cytokine release syndrome, previously observed with IL-15-expressing CART cells¹¹, could potentially be overcome by expressing IL-15 through the *NR4A2* promoter. Furthermore, multiplex editing can be incorporated into our approach, to enable the concurrent disruption of genes that can further enhance T cell function, expression of factors with synergistic functions, or that target distinct processes to provide a multipronged approach to enhance therapeutic efficacy. Moreover, our approach could be broadened to

benefit other forms of ACT, both for cancer-related therapies, such as CAR macrophage or NK cells, or other therapeutic contexts, such as T_{reg} therapy for autoimmune diseases. These applications would require similar experiments to identify tissue-restricted promoters in these cell types to enable localized payload expression.

In summary, by repurposing endogenous gene regulatory mechanisms to express proinflammatory payloads in a tumour-localized manner, we propose that this system will expand the arsenal of proinflammatory factors that can be safely expressed by armoured T cells. We think our approach will broaden the therapeutic reach of ACT by effectively addressing the key challenges of treating solid tumours, including immunosuppression and tumour heterogeneity.

Online content

Any methods, additional references, Nature Portfolio reporting summaries, source data, extended data, supplementary information, acknowledgements, peer review information; details of author contributions and competing interests; and statements of data and code availability are available at <https://doi.org/10.1038/s41586-025-09212-7>.

1. Albelda, S. M. CART cell therapy for patients with solid tumours: key lessons to learn and unlearn. *Nat. Rev. Clin. Oncol.* <https://doi.org/10.1038/s41571-023-00832-4> (2023).
2. Majzner, R. G. & Mackall, C. L. Clinical lessons learned from the first leg of the CART cell journey. *Nat. Med.* **25**, 1341–1355 (2019).
3. Mardiana, S., Solomon, B. J., Darcy, P. K. & Beavis, P. A. Supercharging adoptive T cell therapy to overcome solid tumor-induced immunosuppression. *Sci. Transl. Med.* **11**, eaaw2293 (2019).
4. Chmielewski, M. & Abken, H. TRUCKS, the fourth-generation CAR T cells: current developments and clinical translation. *Adv. Cell Gene Ther.* <https://doi.org/10.1002/acgt.2024> (2020).
5. Zhang, L. et al. Tumor-infiltrating lymphocytes genetically engineered with an inducible gene encoding interleukin-12 for the immunotherapy of metastatic melanoma. *Clin. Cancer Res.* **21**, 2278–2288 (2015).
6. Cappell, K. M. & Kochenderfer, J. N. Long-term outcomes following CAR T cell therapy: what we know so far. *Nat. Rev. Clin. Oncol.* **20**, 359–371 (2023).
7. Zhang, Q. et al. A human orthogonal IL-2 and IL-2R β system enhances CAR T cell expansion and antitumor activity in a murine model of leukemia. *Sci. Transl. Med.* **13**, eabg6986 (2021).
8. Allen, G. M. et al. Synthetic cytokine circuits that drive T cells into immune-excluded tumors. *Science* **378**, eaba1624 (2022).
9. Pegram, H. J. et al. Tumor-targeted T cells modified to secrete IL-12 eradicate systemic tumors without need for prior conditioning. *Blood* **119**, 4133–4141 (2012).
10. Chmielewski, M., Kopecky, C., Hombach, A. O. & Abken, H. IL-12 release by engineered T cells expressing chimeric antigen receptors can effectively muster an antigen-independent macrophage response on tumor cells that have shut down tumor antigen expression. *Cancer Res.* **71**, 5697–5706 (2011).
11. Steffin, D. et al. Interleukin-15-armoured GPC3 CART cells for patients with solid cancers. *Nature* **637**, 940–946 (2025).
12. Avanzi, M. P. et al. Engineered tumor-targeted T cells mediate enhanced anti-tumor efficacy both directly and through activation of the endogenous immune system. *Cell Rep.* **23**, 2130–2141 (2018).
13. Chmielewski, M. & Abken, H. CART T cells releasing IL-18 convert to T-bet^{high} FoxO1^{low} effectors that exhibit augmented activity against advanced solid tumors. *Cell Rep.* **21**, 3205–3219 (2017).

14. Lai, J. et al. Adoptive cellular therapy with T cells expressing the dendritic cell growth factor Flt3L drives epitope spreading and antitumor immunity. *Nat. Immunol.* **21**, 914–926 (2020).

15. Ma, L. et al. Vaccine-boosted CAR T crosstalk with host immunity to reject tumors with antigen heterogeneity. *Cell* **186**, 3148–3165 (2023).

16. Adachi, K. et al. IL-7 and CCL19 expression in CAR-T cells improves immune cell infiltration and CAR-T cell survival in the tumor. *Nat. Biotechnol.* **36**, 346–351 (2018).

17. Zhang, L. et al. Improving adoptive T cell therapy by targeting and controlling IL-12 expression to the tumor environment. *Mol. Ther.* **19**, 751–759 (2011).

18. Roybal, K. T. et al. Engineering T cells with customized therapeutic response programs using synthetic Notch receptors. *Cell* **167**, 419–432 (2016).

19. Hyrenius-Wittsten, A. et al. SynNotch CAR circuits enhance solid tumor recognition and promote persistent antitumor activity in mouse models. *Sci. Transl. Med.* **13**, eabd8836 (2021).

20. Alsaeedi, A., Holler, A., Velica, P., Bendle, G. & Stauss, H. J. Safety and efficacy of Tet-regulated IL-12 expression in cancer-specific T cells. *Oncoimmunology* **8**, 1542917 (2018).

21. Kunert, A. et al. Intra-tumoral production of IL18, but not IL12, by TCR-engineered T cells is non-toxic and counteracts immune evasion of solid tumors. *Oncoimmunology* **7**, e1378842 (2019).

22. Liu, Y. et al. Armored inducible expression of IL-12 enhances antitumor activity of glypican-3-targeted chimeric antigen receptor-engineered T cells in hepatocellular carcinoma. *J. Immunol.* **203**, 198–207 (2019).

23. Eyuquem, J. et al. Targeting a CAR to the TRAC locus with CRISPR/Cas9 enhances tumour rejection. *Nature* **543**, 113–117 (2017).

24. Dai, X. et al. One-step generation of modular CAR-T cells with AAV-Cpf1. *Nat. Methods* **16**, 247–254 (2019).

25. Wiebking, V. et al. Genome editing of donor-derived T-cells to generate allogeneic chimeric antigen receptor-modified T cells: optimizing αβ T cell-depleted haploidentical hematopoietic stem cell transplantation. *Haematologica* <https://doi.org/10.3324/haematol.2019.233882> (2021).

26. Conlon, K. C., Miljkovic, M. D. & Waldmann, T. A. Cytokines in the treatment of cancer. *J. Interferon Cytokine Res.* **39**, 6–21 (2019).

27. Waldmann, T. A. Cytokines in cancer immunotherapy. *Cold Spring Harb. Perspect. Biol.* **10**, a028472 (2018).

28. Kearney, C. J. et al. Tumor immune evasion arises through loss of TNF sensitivity. *Sci. Immunol.* **3**, eaar3451 (2018).

29. Mardiana, S. et al. A multifunctional role for adjuvant anti-4-1BB therapy in augmenting antitumor response by chimeric antigen receptor T cells. *Cancer Res.* **77**, 1296–1309 (2017).

30. Giuffrida, L. et al. IL-15 preconditioning augments CAR T cell responses to checkpoint blockade for improved treatment of solid tumors. *Mol. Ther.* <https://doi.org/10.1016/j.yjmthe.2020.07.018> (2020).

31. Sampson, J. H. et al. EGFRvIII mCAR-modified T-cell therapy cures mice with established intracerebral glioma and generates host immunity against tumor-antigen loss. *Clin. Cancer Res.* **20**, 972–984 (2014).

32. Yang, J. C. & Perry-Lalley, D. The envelope protein of an endogenous murine retrovirus is a tumor-associated T-cell antigen for multiple murine tumors. *J. Immunother.* **23**, 177–183 (2000).

33. Zheng, L. et al. Pan-cancer single-cell landscape of tumor-infiltrating T cells. *Science* **374**, abe6474 (2021).

34. Kleinjan, D. A. & van Heyningen, V. Long-range control of gene expression: emerging mechanisms and disruption in disease. *Am. J. Hum. Genet.* **76**, 8–32 (2005).

35. Schoenfelder, S. & Fraser, P. Long-range enhancer-promoter contacts in gene expression control. *Nat. Rev. Genet.* **20**, 437–455 (2019).

36. Uchibori, R. et al. Functional analysis of an inducible promoter driven by activation signals from a chimeric antigen receptor. *Mol. Ther. Oncolytics* **12**, 16–25 (2019).

37. Guo, T., Ma, D. & Lu, T. K. Sense-and-respond payload delivery using a novel antigen-inducible promoter improves suboptimal CAR-T activation. *ACS Synth. Biol.* **11**, 1440–1453 (2022).

38. Chen, J. et al. NR4A transcription factors limit CAR T cell function in solid tumours. *Nature* **567**, 530–534 (2019).

39. Seo, H. et al. TOX and TOX2 transcription factors cooperate with NR4A transcription factors to impose CD8⁺ T cell exhaustion. *Proc. Natl. Acad. Sci. USA* **116**, 12410–12415 (2019).

40. Weisshaar, N. et al. Rgs16 promotes antitumor CD8⁺ T cell exhaustion. *Sci. Immunol.* **7**, eabhb1873 (2022).

41. Lu, Y. et al. Safety and feasibility of CRISPR-edited T cells in patients with refractory non-small-cell lung cancer. *Nat. Med.* **26**, 732–740 (2020).

42. Stadtmauer, E. A. et al. CRISPR-engineered T cells in patients with refractory cancer. *Science* **367**, eaba7365 (2020).

43. Herbertson, R. A. et al. Phase I biodistribution and pharmacokinetic study of Lewis Y-targeting Immunoconjugate CMD-193 in patients with advanced epithelial cancers. *Clin. Cancer Res.* **15**, 6709–6715 (2009).

44. Scott, A. M. et al. A phase I biodistribution and pharmacokinetic trial of humanized monoclonal antibody Hu3193 in patients with advanced epithelial cancers that express the Lewis-Y antigen. *Clin. Cancer Res.* **13**, 3286–3292 (2007).

45. Ritchie, D. S. et al. Persistence and efficacy of second generation CAR T cell against the LeY antigen in acute myeloid leukemia. *Mol. Ther.* **21**, 2122–2129 (2013).

46. Wu, H.-T. et al. The tumor suppressive roles and prognostic values of STEAP family members in breast cancer. *BioMed. Res. Int.* **2020**, 9578484 (2020).

47. Yang, Q., Ji, G. & Li, J. STEAP2 is down-regulated in breast cancer tissue and suppresses PI3K/AKT signaling and breast cancer cell invasion in vitro and in vivo. *Cancer Biol. Ther.* **21**, 278–291 (2020).

48. Moek, K. L., Fehrmann, R. S. N., van der Vegt, B., de Vries, E. G. E. & de Groot, D. J. A. Glycan 3 overexpression across a broad spectrum of tumor types discovered with functional genomic mRNA profiling of a large cancer database. *Am. J. Pathol.* **188**, 1973–1981 (2018).

49. Sek, K. et al. Tumor site-directed A1R expression enhances CAR T cell function and improves efficacy against solid tumors. *Nat. Commun.* <https://doi.org/10.1038/s41467-025-59021-9> (2025).

Publisher's note Springer Nature remains neutral with regard to jurisdictional claims in published maps and institutional affiliations.



Open Access This article is licensed under a Creative Commons Attribution-NonCommercial-NoDerivatives 4.0 International License, which permits any non-commercial use, sharing, distribution and reproduction in any medium or format, as long as you give appropriate credit to the original author(s) and the source, provide a link to the Creative Commons licence, and indicate if you modified the licensed material. You do not have permission under this licence to share adapted material derived from this article or parts of it. The images or other third party material in this article are included in the article's Creative Commons licence, unless indicated otherwise in a credit line to the material. If material is not included in the article's Creative Commons licence and your intended use is not permitted by statutory regulation or exceeds the permitted use, you will need to obtain permission directly from the copyright holder. To view a copy of this licence, visit <http://creativecommons.org/licenses/by-nc-nd/4.0/>.

© The Author(s) 2025

Methods

Human samples

Buffy coats from healthy donors less than 35 years old were obtained from the Red Cross with informed consent, as approved by the Red Cross and the Peter MacCallum Cancer Centre (PMCC) Human Research and Ethics Committee under HREC#01/14. Frozen apheresis samples were collected from one multiple myeloma patient and six DLBCL patients enrolled in CAR T cell clinical trials. All patients gave informed consent, in accordance with the PMCC Human Research and Ethics Committee under HREC/74245/PMCC.

Animal models

OT-I and C57BL/6 human-Her2 (hHer2) transgenic mice^{50,51} were bred at PMCC. C57BL/6 wild-type mice were purchased from the Walter and Eliza Hall Institute or Australian Bioresources. The Ly5.1 congenic mice and NOD.Cg-Prkdc scid IL2rg (NSG) mice were either bred at PMCC or purchased from Australian Bioresources. The OT-3 mice were bred at the Peter Doherty Institute. All murine experiments were done with mice 6–18 weeks of age and housed in a PC2 specific pathogen-free animal facility, in accordance with the PMCC Animal Experimentation Ethics Committee under projects #E582, #E664, #E671 and #E693, and a minimum of three mice per group were used in each experiment. Mice were randomized before treatment according to tumour size to ensure that all groups had equivalent tumour burdens before therapy. Experiments were not blinded because the same investigators performed and analysed experiments, so blinding was not possible. All experiments complied with the ethical endpoints stated in the approved projects, including maximum tumour size.

Cell lines

All murine tumour cell lines were from a C57BL/6 background. The murine breast carcinoma cell lines AT-3 and E0771 were obtained from T. Stewart (PMCC) and R. Anderson (Olivia Newton-John Cancer Centre), respectively. The murine MC38 colon adenocarcinoma cell line and 24JK sarcoma cell line were provided by J. Schlom (National Institutes of Health) and P. Hwu (National Institutes of Health), respectively. The parental tumour cell lines were retrovirally transduced with a murine stem cell virus vector to obtain hHer2- and ova-expressing tumour cell lines. The human ovarian cancer cell line OVCAR-3 and breast cancer cell lines MCF-7 and MDA-MB-231 were obtained from the American Type Culture Collection. The retroviral packaging lines GP+e86 and PG13, as well as HEK293T, were obtained from the American Type Culture Collection. All cell lines were confirmed to be mycoplasma-negative by polymerase chain reaction (PCR)-based testing.

The E0771, MC38, 24JK, OVCAR-3, MCF-7, GP+e86 and PG13 cell lines were cultured in Roswell Park Memorial Institute (RPMI) 1640 medium supplemented with 10% heat-inactivated fetal bovine serum (FBS), 1 mM sodium pyruvate, 2 mM glutamine, 0.1 mM non-essential amino acids, 10 mM 4-(2-hydroxyethyl)-1-piperazineethanesulfonic acid (HEPES), 100 U ml⁻¹ penicillin and 100 µg ml⁻¹ streptomycin (complete RPMI), and maintained in a humidified incubator at 37 °C with 5% CO₂. The AT-3, MDA-MB-231 and HEK293T cell lines were cultured in Dulbecco's Modified Eagle Medium (DMEM) supplemented with 10% heat-inactivated FBS and maintained in a humidified incubator at 37 °C with 10% CO₂.

Antibodies and cytokines

Murine anti-CD3 (clone 145-2C11) and anti-CD28 (clone 37.51) antibodies were purchased from BD Biosciences. The human anti-CD3 antibody (clone OKT3) was purchased from BioLegend. The anti-Myc tag antibody (clone 9B11) was purchased from Cell Signaling Technology. The anti-LeY idiotype antibody hu3S193 was provided by A. Scott (Olivia Newton-John Cancer Centre)⁵². The recombinant human IL-2 (hIL-2) was obtained from the National Institutes of Health or purchased from

PeproTech and Miltenyi Biotec. The recombinant murine IL-7 (mIL-7) and human IL-15 (hIL-15) were purchased from PeproTech.

CRISPR/Cas9 editing of primary T cells

Murine T cells were activated from naive splenocytes by culturing in complete RPMI containing murine anti-CD3 (0.5 µg ml⁻¹), murine anti-CD28 (0.5 µg ml⁻¹), hIL-2 (100 IU ml⁻¹) and mIL-7 (200 pg ml⁻¹) for 24 h. Human T cells were activated by isolating peripheral blood mononuclear cells from healthy buffy coats and culturing in complete RPMI containing human anti-CD3 (30 ng ml⁻¹) and hIL-2 (600 IU ml⁻¹) for 48 h. To perform CRISPR/Cas9 editing, 37 pmol recombinant Cas9 (IDT) and 270 pmol single guide RNA (sgRNA; Synthego) were combined and incubated at room temperature for 10 min to form Cas9/sgRNA ribonucleoprotein (RNP) complexes. Then, 20 × 10⁶ murine T cells or 1 × 10⁶ human T cells were resuspended in 20 µl P3 electroporation buffer (containing 82% P3 buffer and 18% Supplement 1; Lonza), combined with RNP and electroporated in 20-µl cuvettes using a 4D-Nucleofector X Unit (Lonza) with pulse code CM137 for murine T cells and EO115 for human T cells. For CRISPR-mediated knockout, 100 µl of prewarmed media was immediately added, and T cells were incubated for 10 min at 37 °C before being transferred to an appropriate culture plate. Knockout efficiency was determined by PCR amplification of regions more than 150 bp around the sgRNA cut site in both mock and CRISPR-edited cells, Sanger sequencing of the PCR amplicons and analysis of sequencing data using the Synthego ICE analysis tool (<https://ice.editco.bio/#/>). For CRISPR-mediated knock-in, T cells were immediately washed out with prewarmed media to a concentration of 50 × 10⁶ cells per millilitre and added to an appropriate culture plate containing a mixture of AAV6 at a multiplicity of infection (MOI) of 10,000–100,000 and 2 µM M3814 (MedChemExpress). T cells were incubated at 37 °C for 4 h before AAV6 and M3814 were washed off and downstream protocols were performed. The sgRNA sequences used are included in Supplementary Table 4. Homologous repair templates were manufactured and cloned by NotI digest into pAAV-MCS (Agilent Technologies) by Genscript, and the resulting plasmids were packaged into AAV6 vectors by Vigene Biosciences (now Charles River Laboratories) or PackGene Biotech. The pAAV-MCS was provided by V. Wiebking and M. Porteus (Stanford University), and the homologous repair template sequences used are included in Supplementary Table 5.

Generation of murine and human CAR T cells

Retroviral supernatants were collected from the GP+e86 or PG13 packaging line for transduction of murine T cells with an anti-hHer2 CAR or human T cells with an anti-LeY CAR as previously described^{53–55}. For the generation of GP+e86 or PG13 packaging lines encoding both an anti-hHer2 CAR or anti-LeY CAR and an NFAT promoter⁵⁶ inducing GFP or IL-12 expression, NFAT–GFP or NFAT–IL-12 sequences were cloned into the murine stem cell virus vector encoding a truncated human nerve growth factor receptor, the vector was transfected into GP+e86 or PG13 packaging lines encoding an anti-hHer2 CAR or anti-LeY CAR, and the resulting packaging lines were sorted on nerve growth factor receptor by flow cytometry. Lentiviral transduction was used for the generation of human anti-Her2 CAR T cells. In brief, lentiviral packaging plasmids (pCMV-VSV-G, pMDLg/pRRE, pRSV-Rev) and a plasmid encoding an anti-Her2 CAR (Genscript) were transfected into HEK293T cells. The resulting lentiviral supernatants were collected on three consecutive days, pooled and centrifuged with Lenti-X Concentrator (Takara Bio) to concentrate the lentivirus. Concentrated lentivirus was directly added to human T cells at a MOI of 0.5 with Lentiboost (Sirion) for transduction. Following transduction, murine T cells were maintained in media containing hIL-2 (100 IU ml⁻¹) and mIL-7 (200 pg ml⁻¹) for in vitro assays or mIL-7 (200 pg ml⁻¹) and hIL-15 (10 ng ml⁻¹) for in vivo applications, and human T cells were maintained in media containing hIL-2 (600 IU ml⁻¹).

In vitro co-culture/stimulation assay

Murine and human T cells were co-cultured with tumour cells at an effector to target (E:T) ratio of 1:1 for 24 h before collection of supernatants and flow cytometry analysis of T cells. For 72-h chronic stimulation assays, supernatant was completely removed at the 24 h and 48 h timepoints and an equivalent number of fresh tumour cells were added. For T cell stimulation with anti-CD3 (0.5 μ g ml⁻¹), anti-CD28 (0.5 μ g ml⁻¹), anti-Myc tag antibody (1:1,000) or anti-LeY idiotype antibody (4.5 μ g ml⁻¹), a U-bottomed 96-well plate was coated with 100 μ l PBS containing the appropriate dilutions of antibody at 37 °C for 2 h before wells were washed twice with 200 μ l PBS and T cells were added.

Chromium-51 release assay

Tumour cells were labelled with ⁵¹Cr by resuspending cell pellets in 50 μ Ci ⁵¹Cr per 1 \times 10⁶ cells and incubating at 37 °C for 1 h. Next, 1 \times 10⁴ ⁵¹Cr-labelled tumour cells were co-cultured with T cells at the indicated E:T ratios. As controls for background and total ⁵¹Cr levels, tumour cells were cultured either alone or with 5% Triton X-100 (Sigma-Aldrich). After a 16-h incubation, the ⁵¹Cr level in the supernatant was measured using the automatic gamma counter Wallac Wizard 1470 (PerkinElmer), and T cell killing was quantified using the following formula: [⁵¹Cr CPM (sample) – ⁵¹Cr CPM (background)]/[⁵¹Cr CPM (total) – ⁵¹Cr CPM (background)], where CPM stands for counts per minute.

Incucyte killing assay

Tumour cells expressing mCherry or GFP were co-cultured with T cells in a 384-well black, optically clear flat-bottomed plate (PerkinElmer) at the indicated E:T ratios. Plates were imaged using the Incucyte SX5 Live-Cell Analysis System every 4 h. The assay was run using the 'adherent cell-by-cell' scan type, using a 10 \times objective lens, with acquisition times of 400 ms and 300 ms for the red and green channels, respectively.

Analysis of cytokine production

Supernatants from the in vitro co-culture and stimulation assays and serum samples from mice were analysed for cytokine concentration using BD Cytometric Bead Array Flex sets for IFN γ , TNF, IL-2, IL-12/IL-23p40 (human) and IL-12p70 (murine) (BD Biosciences). Data were acquired using FACSVerse, FACSCanto II or LSRII (BD Biosciences) and analysed using the FCAP Array v.3 software (BD Biosciences).

Flow cytometry

Cells were incubated in FACS buffer (2% FBS, 2 mM EDTA in PBS) containing a 1:50 dilution of Fc receptor block (2.4G2 antibody, produced in-house) with fluorochrome-conjugated antibodies at 4 °C for 30 min in the dark. After staining, cells were washed twice with FACS buffer before analysis or intracellular staining. For cytoplasmic and intranuclear staining, cells were fixed and permeabilized using a BD Cytofix/Cytoperm Fixation Permeabilization Kit (BD Biosciences) or an eBioscience Foxp3/Transcription Factor Staining Buffer Set (Thermo Fisher Scientific) following the manufacturer's instructions, respectively, before staining with fluorochrome-conjugated antibodies at room temperature for 30 min in the dark. Cells were then washed twice with 1 \times BD Perm/Wash Buffer or eBioscience Permeabilization Buffer (diluted from 10 \times stock) before analysis. Data were acquired on either a FACSCanto II, LSRFortessa X-20, LSR II, FACSymphony A3 or A5 (BD Biosciences), and analysed using FlowJo software (BD Biosciences). Cells were quantified using counting beads (Beckman Coulter) using the following formula: cell events of interest/bead events \times number of beads per sample. FC values calculated from negative mean fluorescence intensity values were set to 0.

Adoptive-transfer experiments

For murine adoptive-transfer experiments, C57BL/6 WT, hHer2 transgenic or Ly5.1 mice were inoculated with 5 \times 10⁵ AT-3-ova or 2 \times 10⁵

E0771-hHer2 in the fourth mammary fat pad orthotopically or 4 \times 10⁵ MC38-hHer2 subcutaneously. Tumours were allowed to establish for eight days (AT-3-ova, MC38-hHer2) or six days (E0771-hHer2) before mice were preconditioned with 0.5 Gy (for AT-3-ova and MC38-hHer2) or 4.0 Gy (E0771-hHer2) total body X-ray irradiation. For human adoptive-transfer experiments, NSG mice were inoculated with 1.25 \times 10⁶ MDA-MB-231 in the fourth mammary fat pad orthotopically, or 5–6 \times 10⁶ OVCAR-3 subcutaneously. Tumours were allowed to establish for 7 days (MDA-MB-231) or 10–16 days (OVCAR-3) before preconditioning with 1 Gy total body X-ray irradiation. Mice were intravenously injected with 0.1–1.5 \times 10⁷ OT-I cells or 2 doses of 0.1–1.0 \times 10⁷ murine or human CAR T cells on consecutive days and intraperitoneally injected with 5 doses of hIL-2 (25,000 IU per dose) on consecutive days. For experiments in NSG mice using IL-12-engineered T cells, all T cell groups were edited to disrupt TCR expression by CRISPR/Cas9-mediated *TRAC* knockout to minimize the risk of graft-versus-host disease.

For tumour growth experiments, tumour area was measured using callipers every 2–4 days until all mice reached an ethical end point. The ethical end point for tumour size was 150 mm².

Ex vivo analysis of immune cells

For ex vivo flow cytometry analyses of the tumour, spleen, tumour dLNs, liver, brain, lung, kidney and bone marrow, tissues were collected on days 7–9 for OT-I and murine CAR T cell experiments, and on days 7–14 for human CAR T cell experiments, unless indicated otherwise. Tumours were processed by mechanical dissociation followed by enzymatic digestion with serum-free DMEM containing 1 mg ml⁻¹ collagenase type IV (Sigma-Aldrich) and 0.02 mg ml⁻¹ DNase I (Sigma-Aldrich) at 37 °C for 30 min with gentle shaking, then filtered through a 70- μ m filter followed by a 35- μ m filter before staining. Spleens were processed by macerating and filtering through a 70- μ m filter, red blood cells were lysed with ACK lysis buffer, then samples were filtered through a 35-mm filter before staining. Tumour dLNs were processed by macerating and filtering through a 70- μ m filter mesh before staining. Livers and brains were processed by macerating and filtering through a 70- μ m filter, immune cells were isolated following density gradient centrifugation in 33% Percoll at 2,000 rpm for 12 min, red blood cells were lysed with ACK lysis buffer, then samples were filtered through a 35- μ m filter before staining. Lungs and kidneys were processed by mechanical dissociation followed by enzymatic digestion with serum-free DMEM containing 1 mg ml⁻¹ collagenase type IV (Sigma-Aldrich) and 0.02 mg ml⁻¹ DNase I (Sigma-Aldrich) at 37 °C for 30 min with gentle shaking, filtered through a 70- μ m filter, red blood cells were lysed with ACK lysis buffer, then samples were filtered through a 35- μ m filter before staining. Bone marrow was processed by using a needle and syringe to flush the inner cavity of the femur with FACS buffer, red blood cells were lysed with ACK lysis buffer, then samples were filtered through a 35- μ m filter before staining.

For experiments requiring ex vivo stimulation, samples were stimulated with either 10 ng ml⁻¹ phorbol 12-myristate 13-acetate (PMA) and 1 μ g ml⁻¹ ionomycin, 200 nM SIINFEKL peptide or a cocktail of 5 μ M MC38 neoantigen peptides (Dpagt1^{mut} SIIVFNLL, Reps1^{mut} AQLANDVVL, Adpgk^{mut} ASMTNMELM) as well as GolgiPlug (BD Biosciences) and GolgiStop (BD Biosciences) at a 1:1,000 or a 1:1,500 dilution, respectively. Samples were incubated at 37 °C for 3 h before staining. For ex vivo co-cultures, tumour cells were seeded at 5 \times 10⁴ cells per well in a flat-bottomed 96-well plate the day before tumour collection. After tumour processing, tumour samples were added to the plate and incubated overnight at 37 °C. On the following day, GolgiPlug and GolgiStop were added, and samples were incubated at 37 °C for 3 h before staining.

For flow cytometry analysis of blood, 200 μ l of blood was collected by either retro-orbital or submandibular bleeds into Eppendorf tubes containing 10 μ l EDTA. Red blood cells were lysed three times using 75 μ l ACK lysis buffer before staining. For serum analyses, blood was centrifuged at 10,000g at 4 °C for 15–20 min and serum was collected for downstream analyses.

Immunofluorescence analysis

C57BL/6 hHer2 transgenic mice were subcutaneously engrafted with 4×10^5 MC38-hHer2 for 8 days before the adoptive transfer of 5×10^6 murine anti-hHer2 CAR T cells. Then, 9 days after adoptive transfer, tumours were collected, embedded in OCT compound (Scigen) in a cryomold, stored at -80°C and sectioned at $10 \mu\text{m}$ per tissue slide.

Tissue slides were fixed with ice-cold methanol at -20°C for 20 min, washed twice with FACS buffer at room temperature for 5 min, blocked with 0.2% bovine serum albumin at room temperature for 5 min, and stained at 4°C overnight with fluorochrome-conjugated antibodies prepared at 1:200 dilution in FACS buffer: anti-CD4 FITC (clone RM4-5) and anti-CD8 Alexa Fluor 594 (clone 53-6.7) from BioLegend. On the following day, tissue slides were washed twice with FACS buffer at room temperature for 5 min, stained with DAPI (Thermo Scientific) at room temperature for 10 min, washed twice with FACS buffer at room temperature for 5 min and coverslipped with VECTASHIELD Antifade Mounting Medium (Vector Laboratories). Immunofluorescence images were acquired using an Olympus DP80 camera on an Olympus BX53 microscope using the cellSens Dimension program and analysed using ImageJ.

3' bulk RNA-seq analysis

RNA-seq libraries were prepared from RNA samples using the Quant-seq 3' mRNA-seq Library Prep Kit for Illumina (Lexogen) following the manufacturer's instructions. Single-end, 75–100 bp RNA-seq short reads were generated by NextSeq sequencing (Illumina) and CASAVA 1.8.2 was subsequently used for base calling. RNA-SeQC v.1.1.7 was used to assess the quality of output⁵⁷, and Cutadapt v.2.1 was used to remove random primer bias and poly-A-tail-derived reads. Sequence alignment against the mouse reference genome mm10 or the human reference genome hg19 was done using HISAT2. Finally, the Rsubread software package 2.10.5 was used to quantify the raw reads of genes defined from Ensembl release 96 (ref. 58). Gene counts were normalized using the trimmed means of M -values method and converted into \log_2 counts per million using the EdgeR v.3.8.5 package^{59,60}. Differential gene expression between groups was derived using the quasi-likelihood F-test statistical test method based on the generalized linear model (glm) framework from EdgeR. Principal component analysis was done on normalized counts based on the most-variable genes. Adjusted P -values were computed using the Benjamini–Hochberg method. All differentially expressed genes were classified as significant based on a false discovery rate cut-off of less than 0.05. MA plots were used to represent differential gene expression between groups. Unbiased GSEA was used on a prereduced list of differentially expressed genes identified by RNA-seq analysis. GSEA was done against Hallmark and C2 (canonical pathways) curated gene sets from the Molecular Signatures Database. Annotated in Fig. 5f and Extended Data Fig. 9a are genes associated with the C2 IL-12 signalling pathway (Gene set IL12_STAT4_PATHWAY).

scRNA-seq analysis

We analysed an scRNA-seq atlas of publicly available and previously published datasets of tumour-infiltrating, healthy tissue and peripheral blood T cells from 21 different cancer types, following previously described methods³³. Data integration was done by per-cell size-factor normalization and per-gene z-score scaling across cells for each dataset. Each dataset was then partitioned into mini-clusters to reduce noise before batch-correction with the Harmony package⁶¹. Seurat was then used to further cluster integrated datasets into meta-clusters. To determine binarized expression of genes of interest across different cancer types above mean expression, the scale and average.cell functions from the sscVis package (<https://github.com/Japrin/sscVis/>) was used, and total frequency of cells from each scRNA-seq dataset was plotted as a box-plot. Numbers of patient samples analysed were as follows: $n = 1$ (blood: BCL; tumour: FTC, OV); $n = 2$ (blood: BRCA, multiple myeloma, CHOL; tumour: AML, BCL); $n = 3$ (tumour: multiple myeloma);

$n = 4$ (tumour: SCC, CHOL); $n = 7$ (tumour: STAD, ESCA); $n = 8$ (tumour: HNSCC); $n = 9$ (tumour: UCEC); $n = 10$ (tumour: RC, THCA, NPC); $n = 11$ (blood: HCC; tumour: BCC); $n = 14$ (tumour: BRCA); $n = 16$ (blood: LC, CRC); $n = 17$ (tumour: HCC); $n = 18$ (tumour: CRC); $n = 22$ (tumour: PACA); $n = 26$ (tumour: LC); $n = 44$ (tumour: MELA).

TCR sequencing analysis

RNA was extracted from processed tumour dLN samples and used for TCR sequencing using the RNeasy kit (Qiagen) and the QIAseq Immune Repertoire RNA Library kit (Qiagen) following the manufacturer's instructions. In brief, RNA was reverse transcribed into cDNA using TCR-specific primers, and unique molecular identifiers were ligated to each double-stranded cDNA molecule. The TCR region was enriched using a set of primers specific to the TCR constant regions and a universal primer complementary to the adaptor. Then, the product was amplified using universal primers that incorporate Illumina sequences and indices. The resulting samples were pooled and sequenced in a MiSeq (Illumina, v.3 chemistry) with paired-end 300-bp reads and a custom sequencing primer (Qiagen). Read processing and analysis were performed using Qiagen's web resources (GeneGlobe Data Analysis Centre, software version 1.0), and clonotype calls and quantity estimates were generated using the IMSEQ software (<http://www.imtools.org>).

Statistical analysis

All statistical analyses were performed using Graphpad Prism. The unpaired and paired student's t -tests were used to determine statistical significance between pairs of data. To determine significance between multiple groups with one independent variable, one-way ANOVA and Tukey's multiple-comparisons test were used. To determine significance between multiple groups of data with two independent variables, a repeated measures two-way ANOVA with the Geisser–Greenhouse correction and Tukey's multiple-comparisons test were used. To determine significance between multiple survival curves, the log-rank Mantel–Cox test was used.

Reporting summary

Further information on research design is available in the Nature Portfolio Reporting Summary linked to this article.

Data availability

The RNA-seq data that support the findings of this study have been deposited in the NCBI Gene Expression Omnibus (GEO) under accession GSE292859. All other data are available from the corresponding authors upon reasonable request. Source data are provided with this paper.

- Wang, L. X. J. et al. Tumor ablation by gene-modified T cells in the absence of autoimmunity. *Cancer Res.* **70**, 9591–9598 (2010).
- Piechocki, M. P., Ho, Y.-S., Pilon, S. & Wei, W.-Z. Human ErbB-2 (Her-2) transgenic mice: a model system for testing Her-2 based vaccines. *J. Immunol.* **171**, 5787–5794 (2003).
- Liu, Z. et al. Generation of anti-idiotype antibodies for application in clinical immunotherapy laboratory analyses. *Hybrid. Hybridomics* **22**, 219–228 (2003).
- Giuffrida, L. et al. CRISPR/Cas9 mediated deletion of the adenosine A2A receptor enhances CAR T cell efficacy. *Nat. Commun.* **12**, 3236 (2021).
- Haynes, N. M. et al. Redirecting mouse CTL against colon carcinoma: superior signaling efficacy of single-chain variable domain chimeras containing TCR- ζ vs Fc ϵ RI- γ . *J. Immunol.* **166**, 182–187 (2001).
- John, L. B. et al. Anti-PD-1 antibody therapy potently enhances the eradication of established tumors by gene-modified T cells. *Clin. Cancer Res.* **19**, 5636–5646 (2013).
- Zimmermann, K. et al. Design and characterization of an “all-in-one” lentiviral vector system combining constitutive anti-GD2 CAR expression and inducible cytokines. *Cancers* **12**, 375 (2020).
- DeLuca, D. S. et al. RNA-SeQC: RNA-seq metrics for quality control and process optimization. *Bioinformatics* **28**, 1530–1532 (2012).
- Zerbino, D. R. et al. Ensembl 2018. *Nucleic Acids Res.* **46**, D754–D761 (2018).
- McCarthy, D. J., Chen, Y. & Smyth, G. K. Differential expression analysis of multifactor RNA-Seq experiments with respect to biological variation. *Nucleic Acids Res.* **40**, 4288–4297 (2012).
- Robinson, M. D., McCarthy, D. J. & Smyth, G. K. edgeR: A Bioconductor package for differential expression analysis of digital gene expression data. *Bioinformatics* **26**, 139–140 (2010).

61. Korsunsky, I. et al. Fast, sensitive and accurate integration of single-cell data with Harmony. *Nat. Methods* **16**, 1289–1296 (2019).

Acknowledgements We acknowledge the Animal Facility, Research Laboratory Support Services (RRID: SCR_025699), the Victorian Centre for Functional Genomics (RRID: SCR_025582), the Genotyping (RRID: SCR_025622), Flow Cytometry (RRID: SCR_025550) and Molecular Genomics Core (RRID: SCR_025695) at PMCC for assistance; and K. Gray and L. Mints-Kotowska for the coordination of patient sample collection and the cryopreservation of patient samples, respectively. This work was funded by a program grant, an ideas grant and a Synergy grant from the National Health and Medical Research Council (NHMRC; grants 1132373, 2026555 and 2012454) and a National Breast Cancer Foundation project grant (IIRS-23-006). A.X.Y.C. was supported by an Australian Government research training program scholarship and a Peter MacCallum Cancer Centre Foundation postgraduate scholarship. K.M.Y. was supported by a University of Melbourne research scholarship. J. Lai was supported by a Cancer Research Institute Irvington postdoctoral fellowship (#CRI 3530). P.A.B. is a CRI Lloyd J. Old STAR (CRI5578) and was supported by a Victorian Cancer Agency Mid-Career fellowship (2021–24). I.G.H. was supported by a Victorian Cancer Agency Early Career fellowship (ECRF20017). P.K.D. was supported by an NHMRC Senior Research fellowship (APP1136680). The Beavis laboratory was funded by a US Department of Defense Breast Cancer Research Program Breakthrough Award Level 1 (#BC200025). We acknowledge the consumer representatives K. Gill, M. Rear and G. Sissing for contributions to the study and research direction of the laboratory.

Author contributions A.X.Y.C., K.M.Y., I.G.H., P.K.D. and P.A.B. designed the experiments, developed the methodology, analysed and interpreted data, and wrote the manuscript.

A.X.Y.C., K.M.Y., J.S.K., K.S., Y.-K.H., P.A.D., J.D.A., I.M., K.L.T., E.B.D., D.N., J.T., C.W.C., T.X.H., K.M.A., M.J.v.E., J.M., J.N.L., M.N.d.M., T.J.C., J.Li, C.S., I.G.H., P.K.D. and P.A.B. performed experiments and acquired data. V.W., A.M.S., L.K.M., J.W., J.O., S.J.H., I.A.P., J. Lai. and M.H.P. provided technical assistance and advice on data analysis and interpretation. I.G.H., P.K.D. and P.A.B. supervised the study and were responsible for coordination and strategy.

Competing interests P.A.B. declares research funding from Bristol-Myers-Squibb. P.K.D. declares research funding from Myeloid Therapeutics, Prescient Therapeutics, Bristol-Myers-Squibb and Juno Therapeutics. I.A.P. declares research funding from AstraZeneca, Bristol-Myers-Squibb and Roche Genentech. The authors declare the following patents related to this work: PCT/AU2021/051219, 'Composition and methods for immunotherapy' (19 October 2021) (A.X.Y.C., I.G.H., P.K.D. and P.A.B.); and PCT/AU2024/050379, 'Compositions & methods for immunotherapy - II' (20 April 2023) (A.X.Y.C., K.M.Y., P.K.D. and P.A.B.). M.H.P. serves on the Scientific Advisory Board of Allogene Therapeutics and Biogen. He is on the Board of Directors and has equity in Kamau Therapeutics and has equity in CRISPR Therapeutics. The remaining authors declare no competing interests.

Additional information

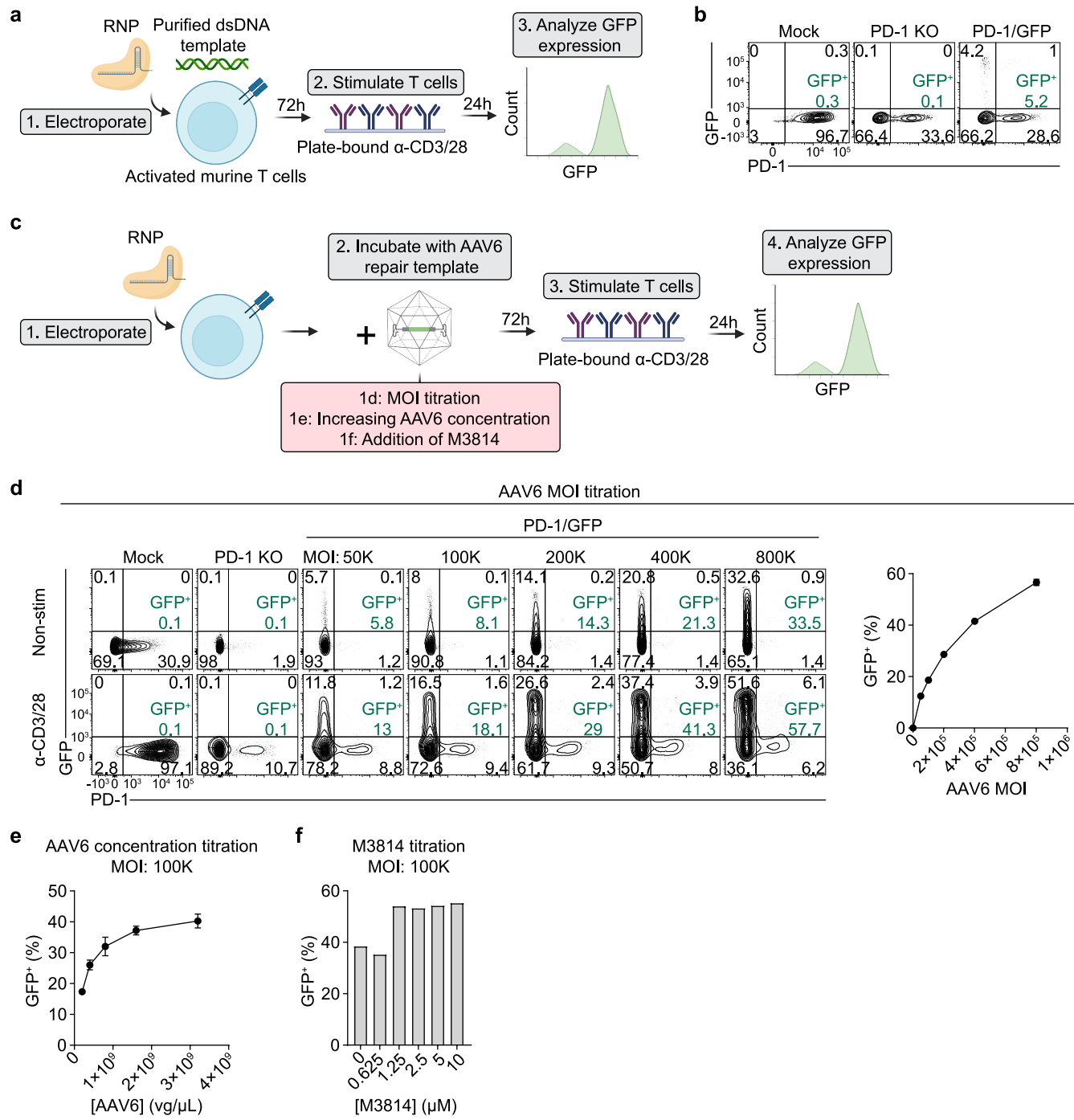
Supplementary information The online version contains supplementary material available at <https://doi.org/10.1038/s41586-025-09212-7>.

Correspondence and requests for materials should be addressed to Amanda X. Y. Chen, Kah Min Yap, Phillip K. Darcy or Paul A. Beavis.

Peer review information *Nature* thanks Steven Albelda and the other, anonymous, reviewer(s) for their contribution to the peer review of this work.

Reprints and permissions information is available at <http://www.nature.com/reprints>.

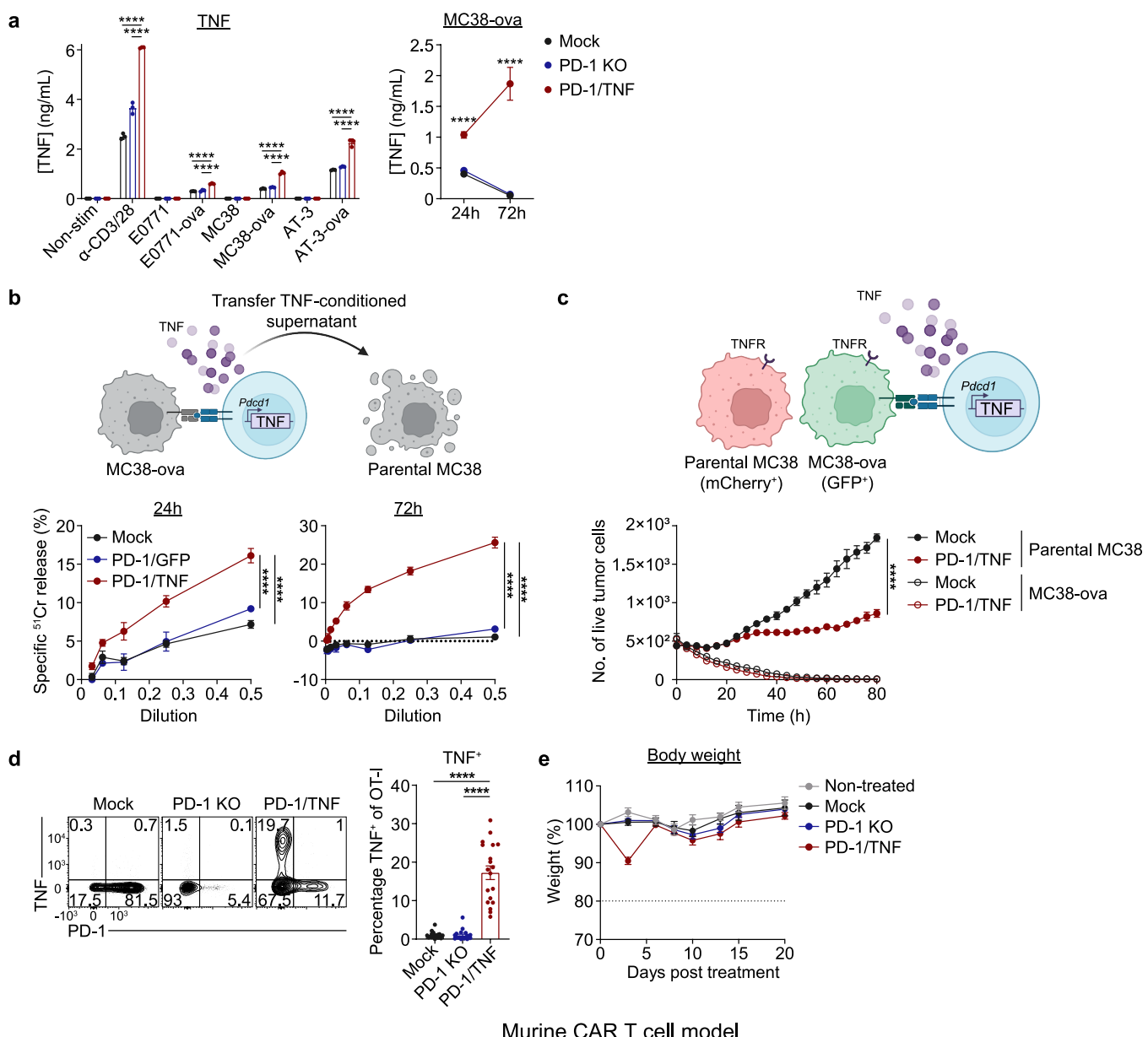
Article



Extended Data Fig. 1 | Optimization of a CRISPR-HDR protocol for engineering primary murine T cells. a. Schematic of CRISPR-HDR protocol using a PD-1/GFP dsDNA repair template. Cas9 and PD-1-targeting sgRNA RNPs were electroporated into activated murine T cells with a purified PD-1/GFP dsDNA repair template and stimulated 72 h later with plate-bound anti-CD3 and CD28 antibodies for 24 h before analysis of GFP by flow cytometry. **b.** Flow cytometry plots showing GFP expression in stimulated Mock, PD-1 KO or PD-1/GFP murine T cells, representative of $n = 3$ experiments. **c.** Schematic of CRISPR-HDR protocol using a PD-1/GFP AAV6 repair template. Cas9 and PD-1-targeting sgRNA RNPs were electroporated into activated murine T cells then incubated with a PD-1/GFP AAV6 repair template for 4 h prior to GFP analyses 72 h later as per (a). **d.** Flow cytometry plots (left) and quantification (right) of

GFP expression in Mock, PD-1KO or PD-1/GFP murine T cells edited with AAV6 at the indicated MOIs. Data represent mean \pm SD of technical duplicates, representative of $n = 2$ experiments. **e.** Quantification of GFP expression in stimulated PD-1/GFP murine T cells edited with AAV6 at an MOI of 100 K, incubated at decreasing volumes to increase the effective AAV6 concentration, represented as mean \pm SD of technical duplicates. **f.** Quantification of GFP expression in stimulated PD-1/GFP murine T cells edited with AAV6 at an MOI of 100 K and M3814 at the indicated concentrations, representative of $n = 2$ experiments. Illustrations in **a** and **c** created using BioRender: **a**, Chen, A., <https://BioRender.com/ye4jk15> (2025); **c**, Chen, A., <https://BioRender.com/ye4jk15> (2025).

OT-I T cell model



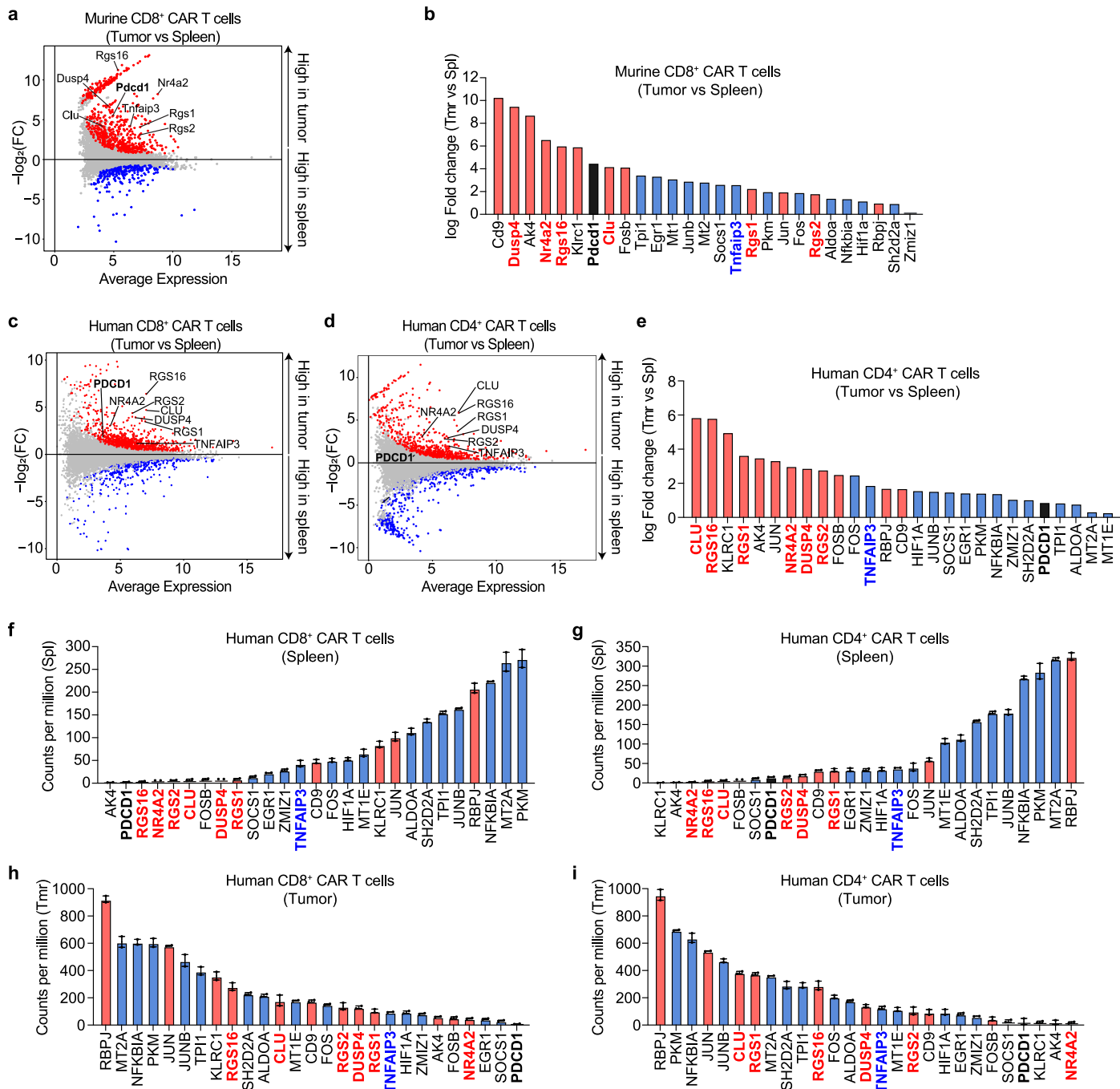
Extended Data Fig. 2 | See next page for caption.

Article

Extended Data Fig. 2 | Validation of CRISPR KI strategy with PD-1/TNF OT-I and murine anti-hHer2 CART cells. **a-e.** Assessment of PD-1/TNF OT-I cells in vitro (**a-c**) and in vivo (**d-e**). **a.** TNF concentration in supernatants of Mock, PD-1 KO or PD-1/TNF OT-I cells stimulated with anti-CD3/28 antibodies or the indicated tumor cell lines for 24 or 72 h. **b.** TNF-conditioned supernatants from a 24 and 72 h coculture with MC38-ova tumor cells and indicated OT-I cells were added to ⁵¹Cr-labelled parental MC38 tumor cells and incubated for 16 h before quantifying ⁵¹Cr release. **c.** OT-I cells were cocultured with a 1:1 mix of mCherry⁺ parental MC38 and GFP⁺ MC38-ova tumor cells and imaged using the Incucyte Live-Cell Analysis System. Tumor cells were quantified based on mCherry or GFP expression. (**a-c**) Data represent mean \pm SD of technical triplicates, representative of $n = 3$ experiments. **d-e.** Mock, PD-1 KO or PD-1/TNF OT-I cells were adoptively transferred into mice bearing orthotopic AT-3-ova tumors. **d.** 8 days post transfer, tumors were harvested, processed and cocultured with fresh AT-3-ova tumor cells for 16 h prior to analysis of TNF expression in OT-I cells.

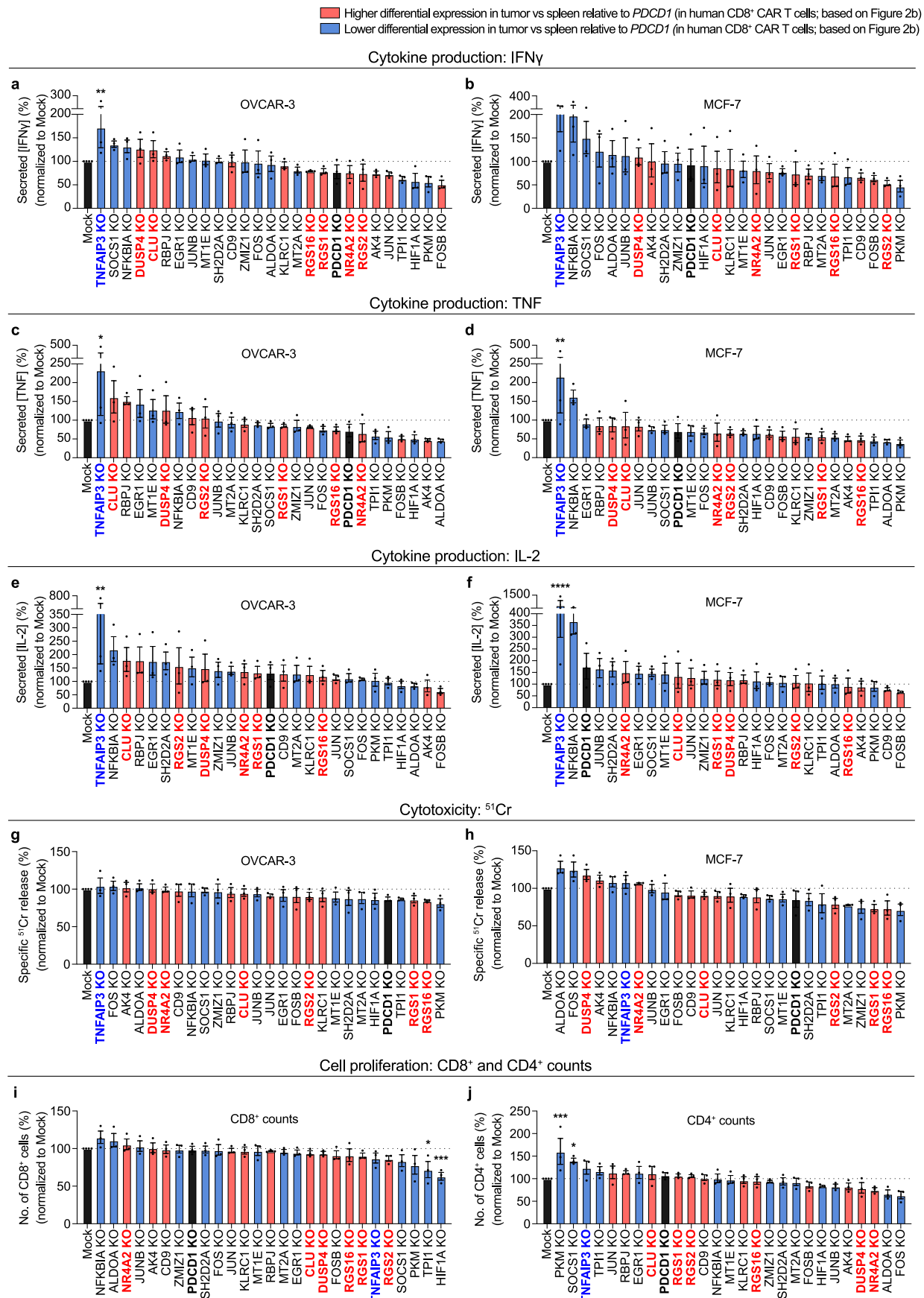
Flow cytometry plots from concatenated samples of $n = 6$ mice/group (left) and quantification of TNF expression represented as mean \pm SEM from $n = 18$ (Mock) and 19 (PD-1 KO, PD-1/TNF) mice/group pooled from $n = 3$ experiments (right). **e.** Body weight of mice, represented as mean \pm SEM from $n = 6$ mice/group. **f-g.** Assessment of PD-1/TNF murine anti-hHer2 CART cells. **f.** TNF concentration in supernatants of Mock, PD-1/GFP or PD-1/TNF murine anti-hHer2 CART cells cocultured with the indicated hHer2-expressing tumor cell lines for 24 h. Data represent mean \pm SD of technical triplicates, representative of $n = 3$ experiments. **g.** Mock, PD-1 KO or PD-1/TNF murine anti-hHer2 CART cells were adoptively transferred into mice bearing subcutaneous MC38-hHer2 tumors. Tumor growth curve represented as mean \pm SEM from $n = 5$ (Non-treated, Mock, PD-1/TNF) and 6 (PD-1 KO) mice/group. (**a-c, f-g**) Two-way ANOVA. (**d**) One-way ANOVA. $*p < 0.05$, $**p < 0.01$, $***p < 0.0001$. Illustrations in **b** and **c** created using BioRender: **b**, Chen, A., <https://BioRender.com/q0g8j7b> (2025); **c**, Chen, A., <https://BioRender.com/q0g8j7b> (2025).

Higher differential expression in tumor vs spleen relative to *PDCD1* (in human CD8⁺ CAR T cells; based on Figure 2b)
Lower differential expression in tumor vs spleen relative to *PDCD1* (in human CD8⁺ CAR T cells; based on Figure 2b)



Extended Data Fig. 3 | RNA sequencing of murine and human CAR T cells isolated from tumors and spleens of tumor-bearing mice. 3' bulk RNA sequencing of CD8⁺ murine anti-hHer2 (a-b) or CD4⁺ (d-e, g, i) or CD8⁺ (c, f, h) human anti-LeY CAR T cells isolated from tumors and spleens of E0771-hHer2 or OVCAR-3 tumor-bearing mice at day 8 or 9 post treatment, respectively. **a.** MA plot depicting differentially expressed genes in CD8⁺ murine CAR T cells isolated from the tumor relative to the spleen. **b.** Log fold change (logFC) in expression in CD8⁺ murine CAR T cells of the top 27 genes identified to exhibit high differential expression in the tumor relative to the spleen in CD8⁺ human CAR T cells from Fig. 2b. Red and blue bars represent genes with higher and

lower logFC than *PDCD1*, respectively. **c-d.** MA plots depicting differentially expressed genes in CD8⁺ (c) or CD4⁺ (d) human CAR T cells isolated from the tumor relative to the spleen. **e.** LogFC in expression in CD4⁺ human CAR T cells of the top 27 genes identified to exhibit high differential expression in the tumor relative to the spleen in CD8⁺ human CAR T cells. **f-i.** Counts per million (CPM) values of the 27 genes in CD8⁺ (f) or CD4⁺ (g) human CAR T cells isolated from the spleen and CD8⁺ (h) or CD4⁺ (i) human CAR T cells isolated from the tumor. (a-i) Data were obtained from $n = 2$ biological replicates, each pooled from $n = 3$ mice.

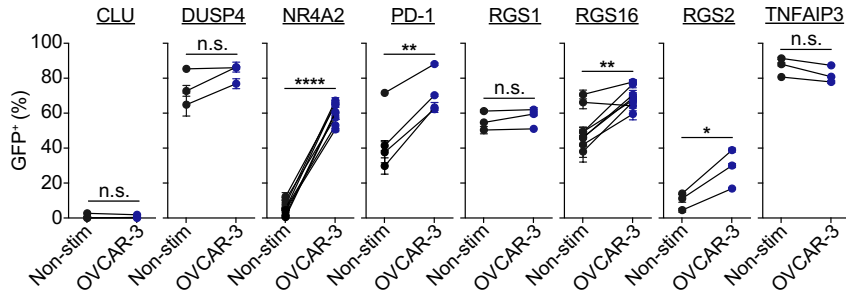


Extended Data Fig. 4 | See next page for caption.

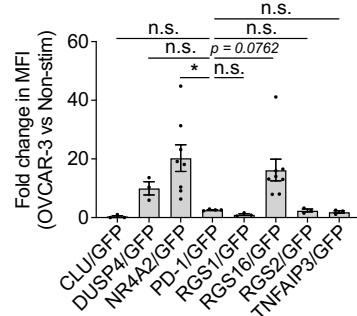
Extended Data Fig. 4 | Impact of CRISPR-mediated knockout of target genes on functions of human anti-LeY CART cells. Each of the 27 target genes of interest was knocked out in human anti-LeY CART cells via CRISPR/Cas9 gene editing. **a-f.** Human CART cells with the indicated gene KO were cocultured with OVCAR-3 (**a, c, e**) or MCF-7 (**b, d, f**) tumor cells for 24 h before the concentrations of IFN γ (**a-b**), TNF (**c-d**) and IL-2 (**e-f**) in supernatants were assessed. **g-h.** Human CART cells with the indicated gene KO were cocultured with ^{51}Cr -labelled OVCAR-3 (**g**) or MCF-7 (**h**) tumor cells for 16 h before quantifying ^{51}Cr release. **i-j.** Human CART cells with the indicated gene KO were maintained in culture with IL-2 for over 28 days and the numbers of CD8 $^{+}$ (**i**) and CD4 $^{+}$ (**j**) T cells were determined. (**a-j**) Data represent logFC values normalized to Mock CART cells pooled from $n = 3$ donors. One-way ANOVA. $*p < 0.05$, $^{**}p < 0.01$, $^{***}p < 0.001$, $^{****}p < 0.0001$.

Article

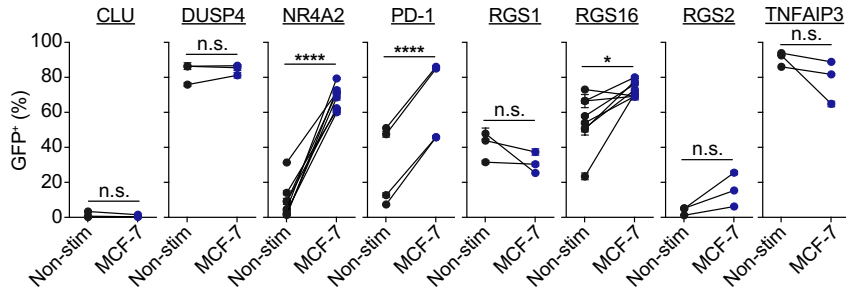
a In vitro tumor coculture: Percentage GFP⁺ of CD4⁺ CAR T cells



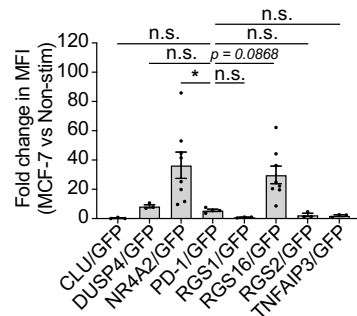
b In vitro tumor coculture: GFP MFI of CD4⁺ CAR T cells



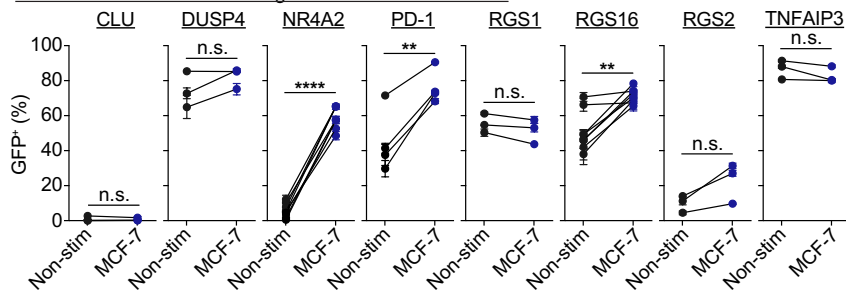
c In vitro tumor coculture: Percentage GFP⁺ of CD8⁺ CAR T cells



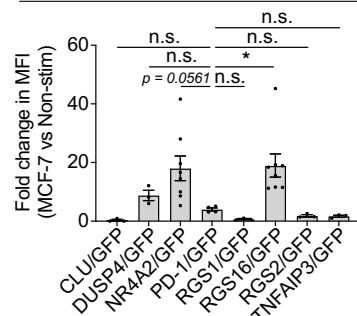
d In vitro tumor coculture: GFP MFI of CD8⁺ CAR T cells



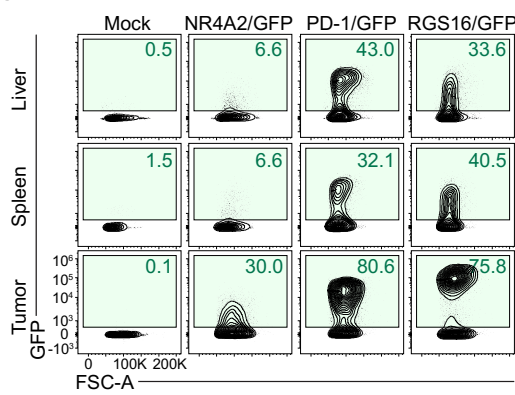
e In vitro tumor coculture: Percentage GFP⁺ of CD4⁺ CAR T cells



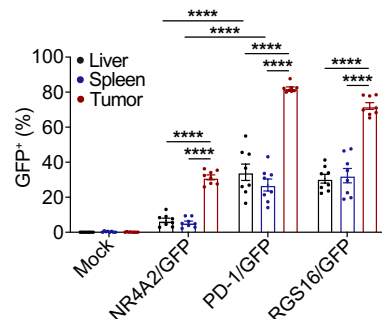
f In vitro tumor coculture: GFP MFI of CD4⁺ CAR T cells



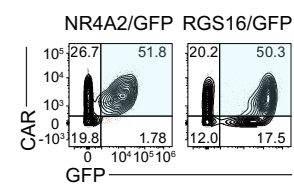
g In vivo: CD8⁺ CAR T cells



h In vivo: Percentage GFP⁺ of CD8⁺ CAR T cells



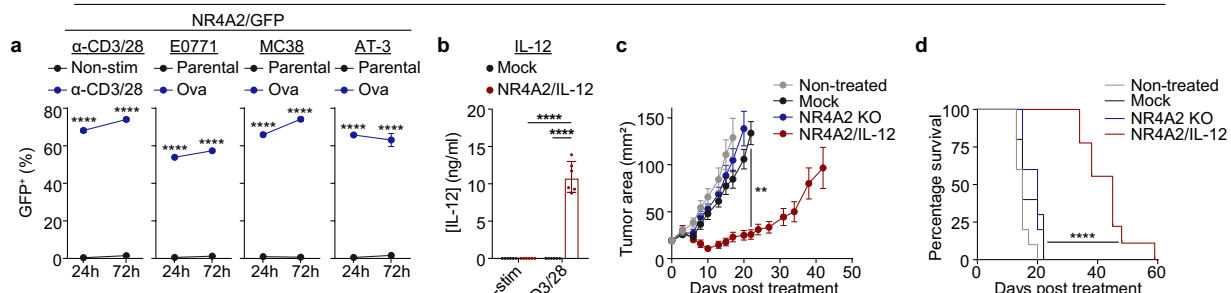
i



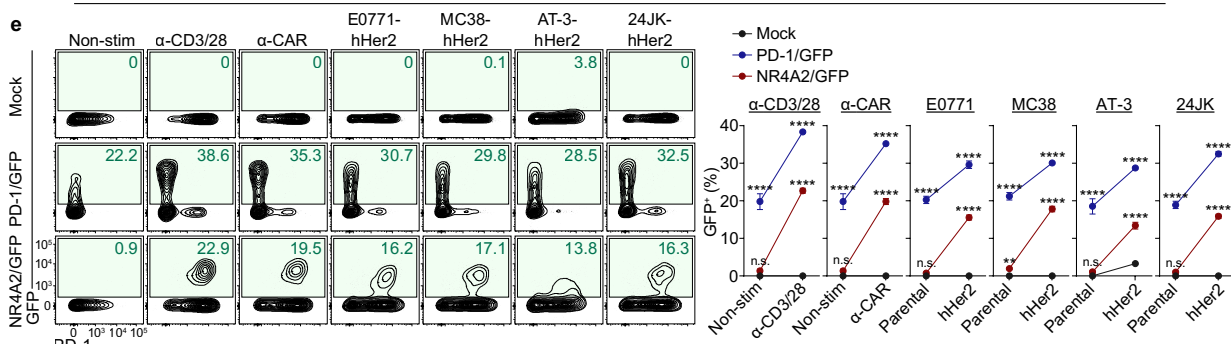
Extended Data Fig. 5 | Transgene expression profiles of shortlisted target genes in human anti-LeY CAR T cells. a-f. Human anti-LeY CAR T cells were engineered to express *Gfp* from the indicated gene loci and cocultured with OVCAR-3 (a-b) or MCF-7 (c-f) tumor cells for 72 h before GFP expression in CD4⁺ (a-b, e-f) or CD8⁺ (c-d) CAR T cells was assessed. a, c, e. Quantification of GFP percentage and b, d, f. fold change in GFP MFI of human CAR T cells following coculture. (a, c, e) Data represent mean \pm SD of technical triplicates from $n = 3$ (CLU, DUSP4, RGS1, RGS2, TNFAIP3), 4 (PD-1) and 8 (NR4A2, RGS16) donors. (b, d, f) Data represent mean \pm SEM pooled from $n = 3$ (CLU, DUSP4, RGS1, RGS2, TNFAIP3), 4 (PD-1) and 8 (NR4A2, RGS16) donors. g-h. Human anti-LeY CAR T cells engineered as per (a-f) were adoptively transferred into mice bearing

subcutaneous OVCAR-3 tumors. 14 days later, tumors, spleens and livers were harvested and GFP expression by CD8⁺ human CAR T cells was assessed. g. Flow cytometry plots from concatenated samples of $n = 4$ mice/group, representative of $n = 2$ donors. h. Quantification of GFP percentage of CD8⁺ human CAR T cells in the tumor, spleen and liver. Data represent mean \pm SEM from $n = 8$ mice/group pooled from $n = 2$ donors. i. Human anti-LeY CAR T cells engineered as per (a-f) were cocultured with OVCAR-3 tumor cells for 72 h. Concatenated flow cytometry plots showing CAR and GFP expression in CD8⁺ T cells from technical triplicates, representative of $n = 8$ donors. (a, c, e) Paired student's t-test. (b, d, f) One-way ANOVA. (h) Two-way ANOVA. n.s. not significant, * $p < 0.05$, ** $p < 0.01$, *** $p < 0.001$.

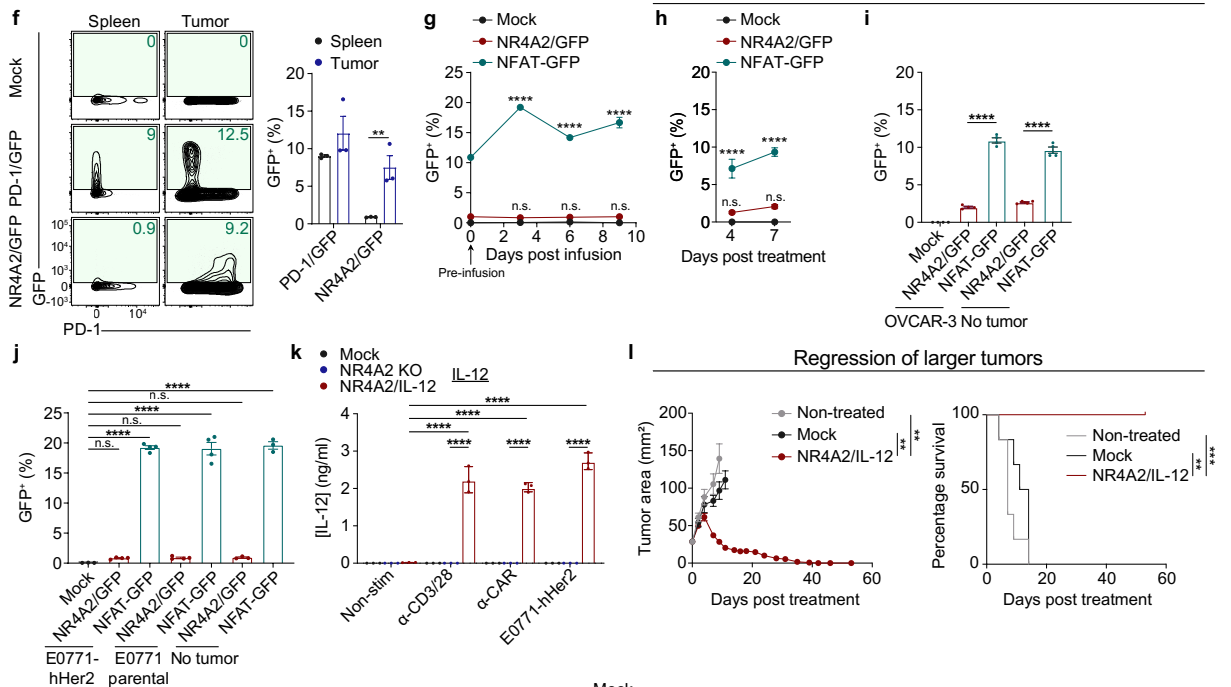
OT-I T cell model



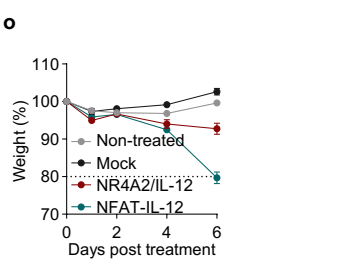
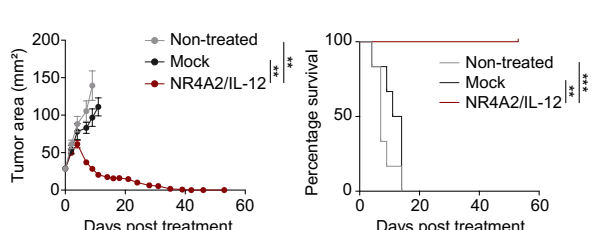
Murine CAR T cell model



Human CAR T cell model



Regression of larger tumors

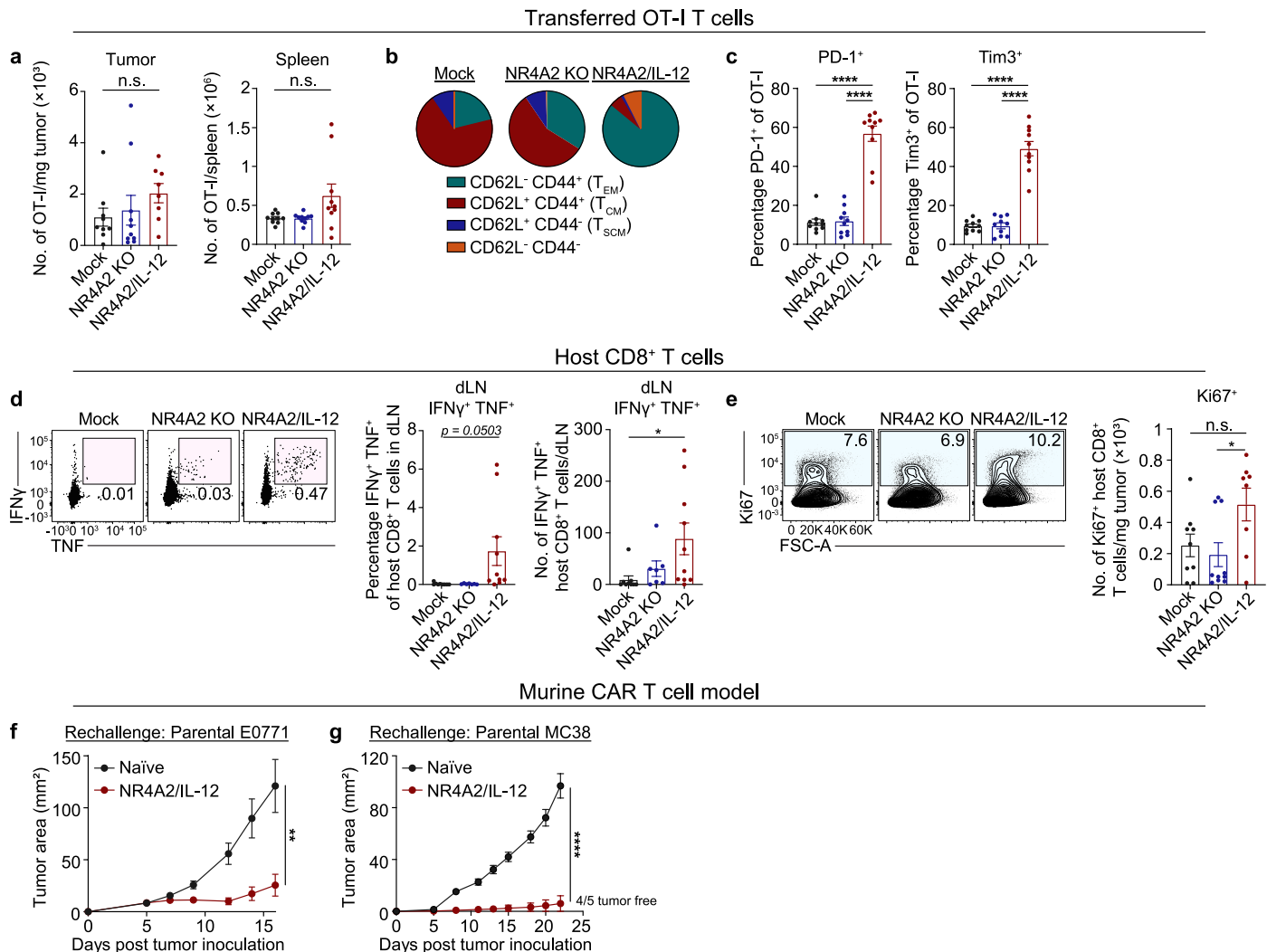


Extended Data Fig. 6 | See next page for caption.

Article

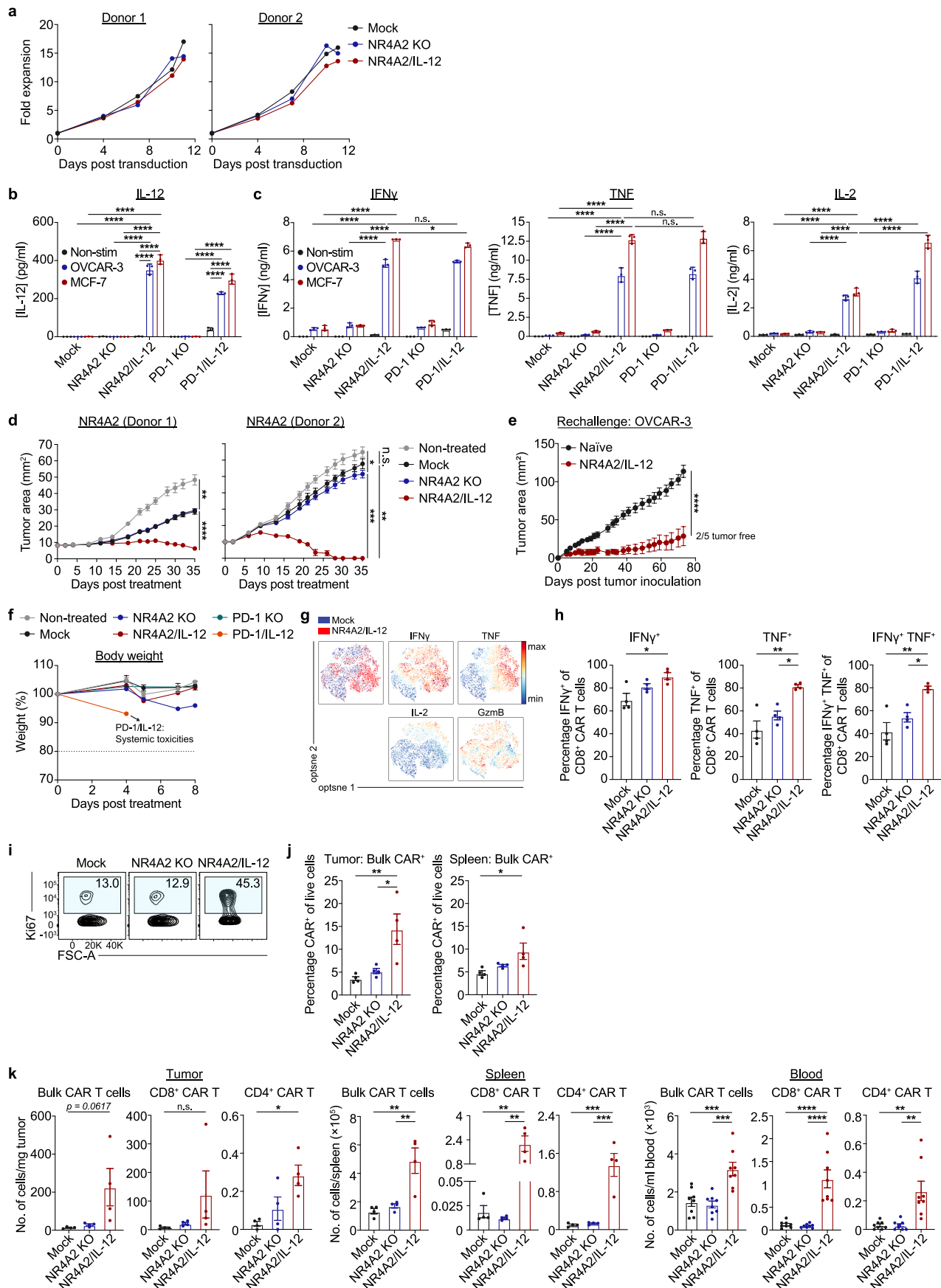
Extended Data Fig. 6 | Assessment of transgene expression driven by the *Nr4a2* and NFAT promoters. **a.** NR4A2/GFP OT-I cells were stimulated with anti-CD3/28 antibodies or the indicated ova-expressing tumor lines for 24 or 72 h before GFP expression was quantified. Data represent mean \pm SD of technical triplicates, representative of $n = 3$ experiments. **b-d.** NR4A2/IL-12 OT-I cells were generated and assessed in vitro (**b**) and in vivo (**c-d**). **b.** IL-12 concentration in supernatants of Mock or NR4A2/IL-12 OT-I cells stimulated with anti-CD3/28 antibodies for 24 h, represented as mean \pm SD of $n = 6$ technical replicates. **c-d.** 1×10^6 Mock, NR4A2 KO or NR4A2/IL-12 OT-I cells were adoptively transferred into mice bearing orthotopic AT-3-ova tumors. **c.** Tumor growth curve represented as mean \pm SEM from $n = 5$ mice/group, representative of $n = 3$ experiments. **d.** Survival curve from $n = 5$ (NR4A2 KO), 9 (NR4A2/IL-12) and 10 (Non-treated, Mock) mice/group, pooled from $n = 2$ experiments. **e-f.** Murine anti-hHer2 CAR T cells were engineered to express *Gfp* via the *Pdcd1* or *Nr4a2* locus and assessed upon in vitro stimulation with anti-CD3/28, anti-CAR antibodies or the indicated tumor cell lines (**e**) and in mice bearing orthotopic E0771-hHer2 tumors (**f**). **e.** Concatenated flow cytometry plots (left) and quantification (right) of GFP expression in CAR T cells following a 24 h stimulation. Data represent mean \pm SD of technical triplicates, representative of $n = 3$ experiments. **f.** Concatenated flow cytometry plots (left) and quantification (right) of GFP percentage in CAR T cells in the tumor and spleen harvested 7 days post transfer. Data represent mean \pm SEM from $n = 3$ mice/group, representative of $n = 2$ experiments. **g.** Murine T cells were retrovirally transduced with an anti-hHer2 CAR and either with an NFAT-GFP construct or CRISPR-engineered to express *Gfp* from the *Nr4a2* locus, and assessed for GFP expression in mice bearing orthotopic E0771-hHer2 tumors. Quantification of GFP percentage in CAR T cells pre-infusion and in the spleen of mice 3, 6 and 9 days post transfer, represented as mean \pm SEM from $n = 3$ (Mock) and 4 (NR4A2/GFP, NFAT-GFP) mice/group. **h-i.** Human T cells were retrovirally transduced with an anti-LeY CAR and either with an NFAT-GFP construct or CRISPR-engineered to express *Gfp* from the *NR4A2* locus, and assessed for GFP expression in mice bearing subcutaneous OVCAR-3 tumors (**h-i**) or non-tumor bearing mice (**i**).

Quantification of GFP percentage in CD8⁺ human CAR T cells in **h**, the blood of tumor-bearing mice 4 and 7 days post transfer and **i**, the spleen of tumor- and non-tumor bearing mice 7 days post transfer, represented as mean \pm SEM from $n = 4$ mice/group. **j.** Murine T cells engineered as per (**g**) were assessed for GFP expression in mice bearing orthotopic E0771-hHer2 tumors, E0771 parental tumors or non-tumor bearing mice. Quantification of GFP percentage in CAR T cells in the spleen of mice 3 days post transfer, represented as mean \pm SEM from $n = 3$ (Mock) and 4 (NR4A2/GFP, NFAT-GFP) mice/group (E0771-hHer2); $n = 4$ mice/group (E0771 parental); $n = 3$ mice/group (no tumor). **k.** IL-12 concentration in supernatants of Mock, NR4A2 KO or NR4A2/IL-12 murine anti-hHer2 CAR T cells stimulated with anti-CD3/28 or anti-CAR antibodies, or E0771-hHer2 tumor cells for 24 h. Data represent mean \pm SD of technical triplicates, representative of $n = 3$ experiments. **l.** 5×10^6 mock or NR4A2/IL-12 murine anti-hHer2 CAR T cells were adoptively transferred into mice bearing orthotopic E0771-hHer2 tumors $> 30 \text{ mm}^2$. Tumor growth curves (left) represented as mean \pm SEM from $n = 6$ mice/group. Survival curves (right) from $n = 6$ mice/group. **m.** 5×10^6 mock, NR4A2 KO or NR4A2/IL-12 murine anti-hHer2 CAR T cells were adoptively transferred into mice bearing orthotopic E0771-hHer2 tumors (left) or subcutaneous MC38-hHer2 tumors (right). Body weights represented as mean \pm SEM from $n = 4$ (NR4A2/IL-12) and 6 (Non-treated, Mock, NR4A2 KO) mice/group (E0771-hHer2); $n = 6$ mice/group (MC38-hHer2). **n-o.** Murine T cells were retrovirally transduced with an anti-hHer2 CAR and either with an NFAT-IL-12 construct or CRISPR-engineered to express IL-12 from the *Nr4a2* locus. **n.** Concentration of IL-12 in supernatants upon in vitro stimulation with anti-CD3/28, anti-CAR antibodies or hHer2-expressing tumor cells. Data represent mean \pm SD of technical triplicates, representative of $n = 2$ experiments. **o.** 5×10^6 mock, NR4A2/IL-12 or NFAT-IL-12 murine anti-hHer2 CAR T cells were adoptively transferred into mice bearing orthotopic E0771-hHer2 tumors. Body weights represented as mean \pm SEM from $n = 5$ (NFAT-IL-12) and 6 (Non-treated, Mock, NR4A2/IL-12) mice/group. **(a-c, e, f-h, j-k, l (left), n)** Two-way ANOVA. **(d, l (right))** Logrank Mantel-Cox test. **(i)** One-way ANOVA. *n.s.* not significant, $^{**}p < 0.01$, $^{***}p < 0.001$, $^{****}p < 0.0001$.



Extended Data Fig. 7 | Mechanistic studies of NR4A2/IL-12 OT-I T cells and murine anti-hHer2 CAR T cells. a-e. NR4A2/IL-12 OT-I T cells (CD45.2⁺) were adoptively transferred into congenic CD45.1⁺ mice bearing orthotopic AT-3-ova tumors and ex vivo analyses were performed 8 days post transfer. Transferred OT-I T cells were identified as live CD45.2⁺ Thy1.2⁺ CD8⁺ cells. Endogenous CD8⁺ T cells were identified as live CD45.1⁺ Thy1.2⁺ CD8⁺ cells. **a.** Quantification of OT-I T cells in the tumor (left) and spleen (right). **b.** Proportion of splenic OT-I T cells with effector memory (T_{EM}), central memory (T_{CM}) or stem cell memory (T_{SCM}) phenotype, based on CD62L and CD44 expression. Data represent mean proportions from $n = 5$ mice/group. **c.** Quantification of PD-1 and Tim3 expression in OT-I T cells in the spleen. **d.** Concatenated flow cytometry plots (left) and quantification (right) of TNF and IFN γ expression in host CD8⁺ T cells in the dLN. **e.** Concatenated flow cytometry plots (left) and quantification (right) of Ki67 expression in host CD8⁺ T cells in the tumor. **(d-e)** Samples were

ex vivo stimulated with SIINFEKL peptide for 3 h. **(a, c-e)** Data represent mean \pm SEM from $n = 8$ (NR4A2/IL-12), 9 (Mock) and 10 (NR4A2 KO) mice/group (tumor), or $n = 10$ mice/group (spleen) **(a)**, $n = 10$ mice/group **(c)**, $n = 7$ (NR4A2 KO), 9 (Mock) and 10 (NR4A2/IL-12) mice/group **(d)**, or $n = 8$ (NR4A2/IL-12), 9 (Mock) and 10 (NR4A2 KO) mice/group **(e)** pooled from $n = 2$ experiments. **(d-e)** Flow cytometry plots from concatenated samples of $n = 5$ mice/group. **f-g.** Mice with previously cured E0771-hHer2 **(f)** or MC38-hHer2 **(g)** tumors following treatment with NR4A2/IL-12 murine anti-hHer2 CAR T cells were rechallenged with parental E0771 or MC38 tumors in the opposite mammary fat pad or flank, respectively. Tumor growth curves represented as mean \pm SEM from $n = 6$ mice/group (E0771) or $n = 5$ (NR4A2/IL-12) and 11 (Naïve) mice/group (MC38). **(a, c-e)** One-way ANOVA. **(f-g)** Two-way ANOVA. *n.s.* not significant, $*p < 0.05$, $**p < 0.01$, $***p < 0.0001$.

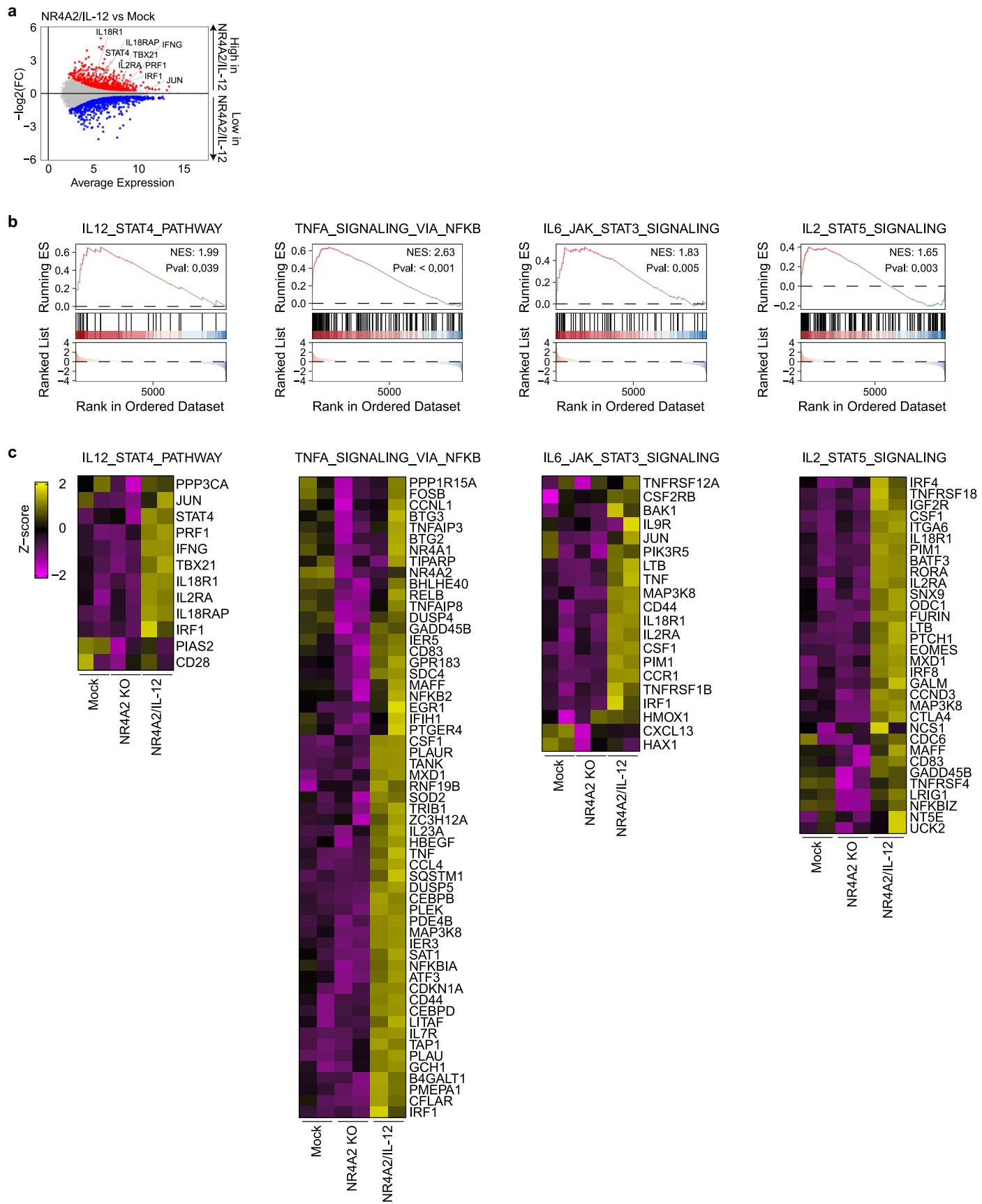


Extended Data Fig. 8 | See next page for caption.

Extended Data Fig. 8 | Scalability, therapeutic efficacy and safety of NR4A2/IL-12 human anti-LeY CAR T cells. **a.** Human anti-LeY CAR T cells engineered to express IL-12 from the *NR4A2* locus were maintained in culture with IL-2 for over 11 days and the fold expansion following transduction was determined from $n = 2$ donors. **b-c.** Human anti-LeY CAR T cells engineered to express IL-12 from either the *NR4A2* or *PDCD1* locus were co-cultured with OVCAR-3 or MCF-7 tumor cells for 24 h before the concentrations of IL-12 (**b**) as well as IFN γ , TNF and IL-2 (**c**) in supernatants were assessed. Data represent mean \pm SD of technical triplicates. **d-k.** Human anti-LeY CAR T cells engineered as per (**b-c**) were adoptively transferred into mice bearing subcutaneous OVCAR-3 tumors. **d.** Tumor growth curves from $n = 2$ donors, represented as mean \pm SEM from $n = 5$ (NR4A2/IL-12) and 6 (Non-treated, Mock, NR4A2 KO) mice/group (Donor 1), or $n = 3$ (NR4A2/IL-12), 4 (Mock, NR4A2 KO) and 6 (Non-treated) mice/group (Donor 2). **e.** Mice with previously cured OVCAR-3 tumors following treatment with NR4A2/IL-12 human anti-LeY CAR T cells were rechallenged with OVCAR-3 tumors in the opposite flank. Tumor growth curves represented as mean \pm SEM from $n = 5$ (NR4A2/IL-12) and 9 (Naïve) mice/group. **f.** Body weight of mice post

treatment, represented as mean \pm SEM from $n = 6$ mice/group. **g-k.** Ex vivo analysis of human CAR T cells isolated from tumors (**g-h, j-k**), spleens (**j-k**) or blood (**i, k**) 11-14 days post transfer. **g.** t-SNE plots comparing expression of indicated proteins in intratumoral Mock and NR4A2/IL-12 CD8 $^{+}$ human CAR T cells, concatenated from $n = 4$ mice/group. **h.** Quantification of IFN γ and TNF expression in intratumoral CD8 $^{+}$ human CAR T cells. Data represent mean \pm SEM from $n = 4$ mice/group. **(g-h)** Tumor samples were ex vivo stimulated with PMA/Ionomycin for 3 h. **i.** Flow cytometry plots showing Ki67 expression in CD8 $^{+}$ human CAR T cells isolated from the blood, concatenated from $n = 5$ (NR4A2/IL-12) and 6 (Mock, NR4A2 KO) mice/group. **j.** Quantification of CAR expression in the tumor and spleen, represented as mean \pm SEM from $n = 4$ mice/group. **k.** Quantification of bulk, CD8 $^{+}$ and CD4 $^{+}$ human CAR T cells isolated from tumors (left), spleens (middle) and blood (right). Left and middle: Data represent mean \pm SEM from $n = 4$ mice/group. Right: Data represent mean \pm SEM from $n = 8$ mice/group, representative of $n = 2$ donors. **(b-c, d-e)** Two-way ANOVA. **(h, j-k)** One-way ANOVA. *n.s.* not significant, $*p < 0.05$, $**p < 0.01$, $***p < 0.001$, $****p < 0.0001$.

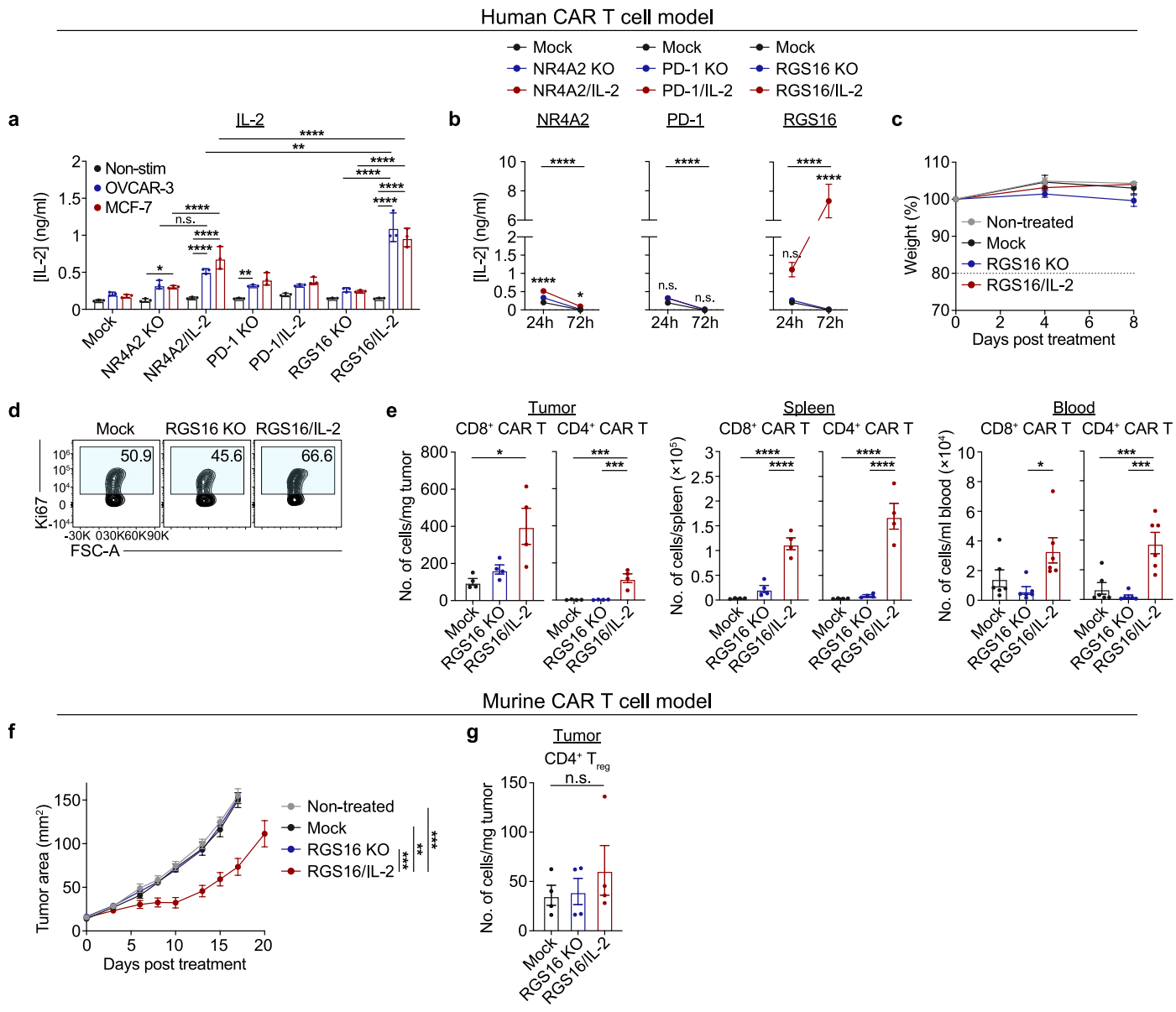
Article



Extended Data Fig. 9 | See next page for caption.

Extended Data Fig. 9 | Transcriptomic analysis of NR4A2/IL-12 human anti-LeY CAR T cells. Human anti-LeY CAR T cells were engineered to express IL-12 from the *NR4A2* locus and adoptively transferred into mice bearing subcutaneous OVCAR-3 tumors. 3' bulk RNA sequencing analysis was performed on CD8⁺ CAR T cells isolated from tumors at day 14 post treatment. **a.** MA plot comparing gene expression in NR4A2/IL-12 and Mock-edited CAR T cells. Annotated genes are those associated with the C2 IL-12 signaling

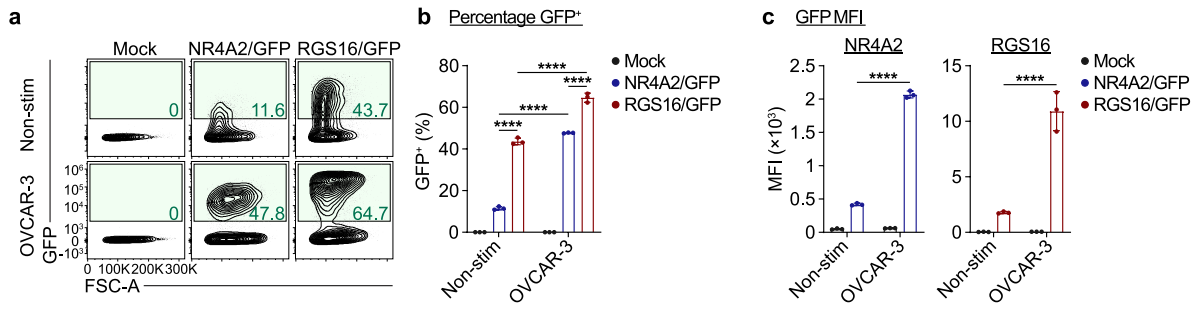
pathway (Gene Set: IL12_STAT4_PATHWAY). **b-c.** Gene set enrichment analysis (GSEA) plots (**b**) and heatmaps (**c**) for C2 (IL12_STAT4_PATHWAY) or Hallmark (TNFA_SIGNALING_VIA_NFKB, IL6_JAK_STAT3_SIGNALING and IL2_STAT5_SIGNALING) pathways determined to exhibit differential expression between NR4A2/IL-12 and NR4A2 KO or Mock-edited CAR T cells. **(a-c)** Data were obtained from $n = 2$ biological replicates per group, each pooled from $n = 8$ mice.



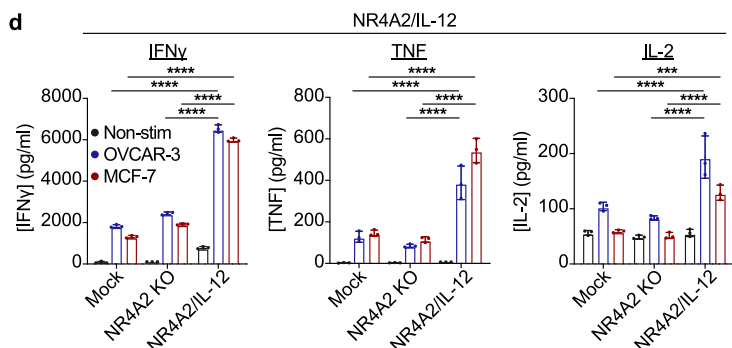
Extended Data Fig. 10 | Characterization of RGS16/IL-2 human anti-LeY and murine anti-hHer2 CAR T cells. a-b. Human anti-LeY CAR T cells were engineered to express IL-2 from either the *NR4A2*, *PDCD1* or *RGS16* locus and co-cultured with OVCAR-3 or MCF-7 tumor cells for 24 and 72 h before the concentration of IL-2 in supernatants was assessed. **a.** Concentration of IL-2 post 24 h of stimulation with OVCAR-3 or MCF-7 tumor cells. **b.** Concentration of IL-2 post 24 and 72 h of stimulation with OVCAR-3 tumor cells. **(a-b)** Data represent mean \pm SD of technical triplicates. **c-e.** Human anti-LeY CAR T cells engineered as per **(a-b)** were adoptively transferred into mice bearing subcutaneous OVCAR-3 tumors. **c.** Body weight of mice post treatment, represented as mean \pm SEM from $n = 6$ mice/group. **d.** Flow cytometry plots of Ki67 expression in intratumoral CD8 $^{+}$ human CAR T cells following ex vivo

stimulation with PMA/Ionomycin for 3 h, concatenated from $n = 4$ mice/group. **e.** Quantification of CD8 $^{+}$ and CD4 $^{+}$ human CAR T cells in tumors (left), spleens (middle) and blood (right) 14–15 days post transfer. Left and middle: Data represent mean \pm SEM from $n = 4$ mice/group. Right: Data represent mean \pm SEM from $n = 6$ mice/group, representative of $n = 2$ donors. **f-g.** 5×10^6 mock, RGS16 KO or RGS16/IL-2 murine anti-hHer2 CAR T cells were adoptively transferred into mice bearing orthotopic E0771-hHer2 tumors. **f.** Tumor growth curves represented as mean \pm SEM from $n = 4$ (RGS16 KO), 5 (Mock) and 6 (Non-treated, RGS16/IL-2) mice/group. **g.** Quantification of intratumoral T $_{reg}$ (CD4 $^{+}$ CD25 $^{+}$ FoxP3 $^{+}$) 9 days post transfer. Data represent mean \pm SEM from $n = 4$ mice/group. **(a-b, f)** Two-way ANOVA. **(e, g)** One-way ANOVA. *n.s.* not significant, $*p < 0.05$, $^{**}p < 0.01$, $^{***}p < 0.001$, $^{****}p < 0.0001$.

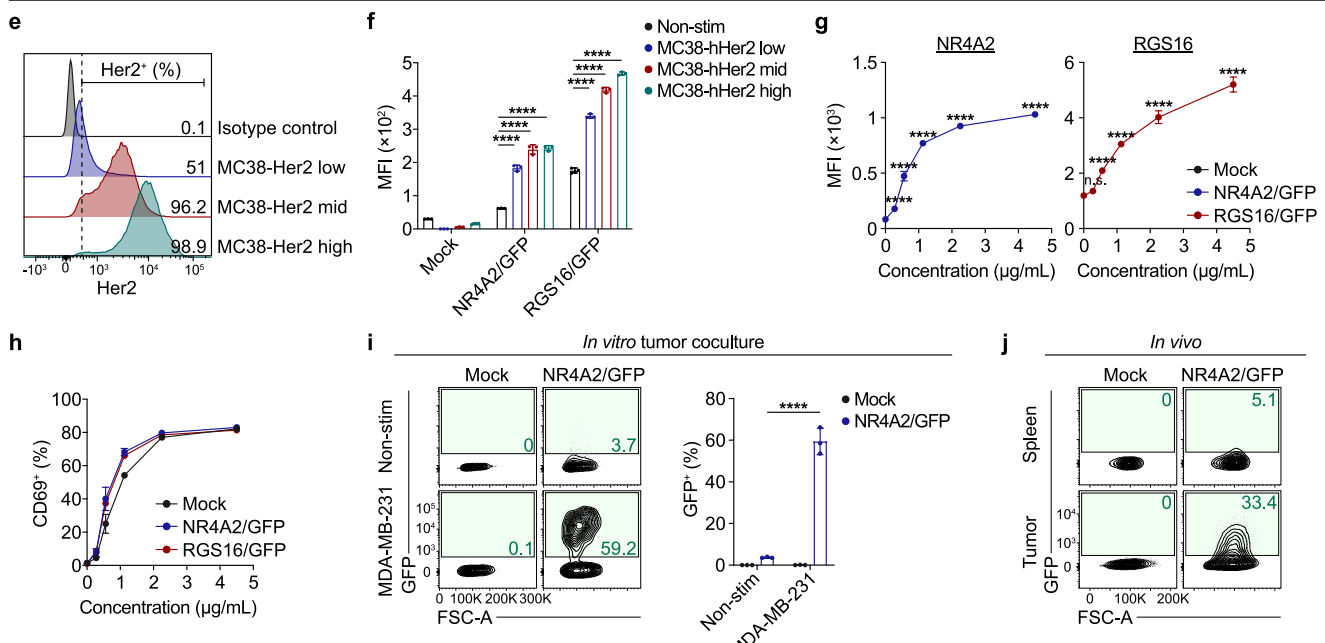
CRISPR-engineered multiple myeloma patient T cells



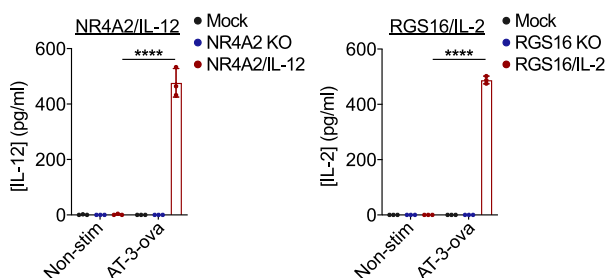
CRISPR-engineered B cell lymphoma patient T cells



Promoter sensitivity across varying antigen densities and affinities



OT-3 T cell model



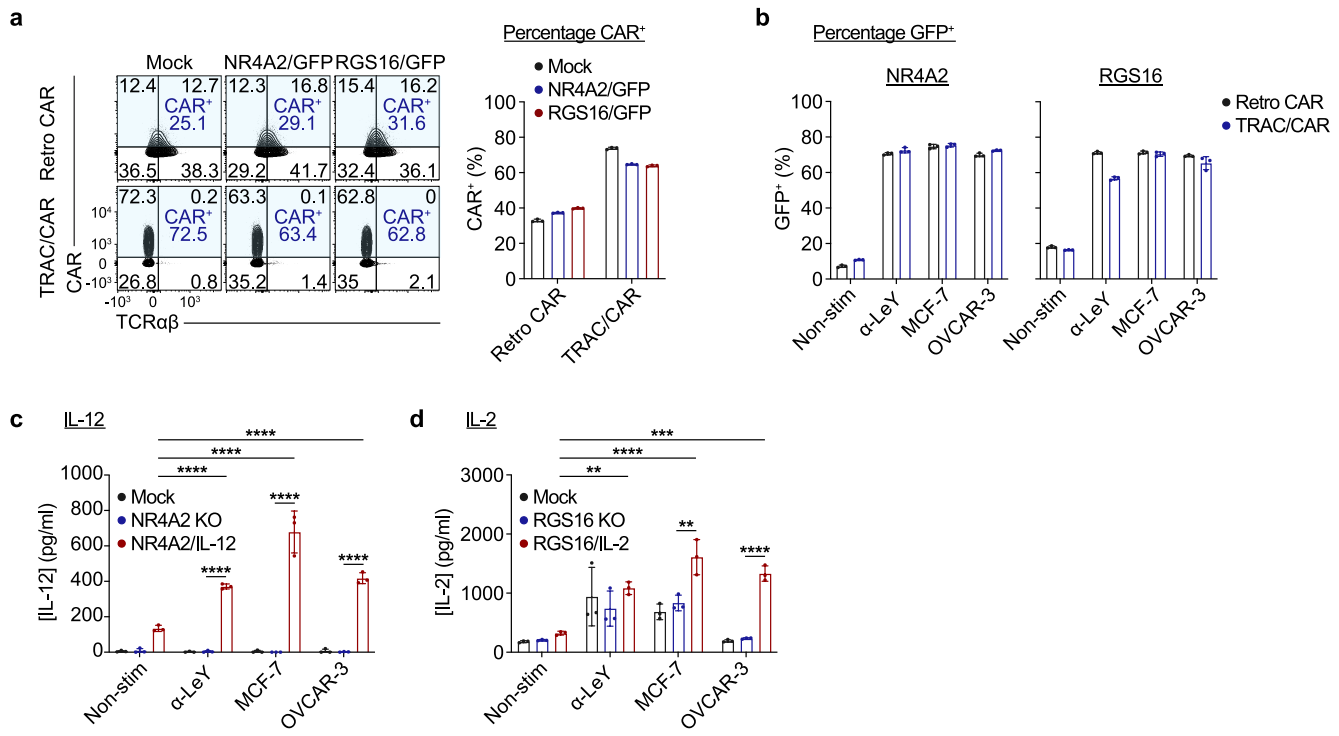
Article

Extended Data Fig. 11 | Clinical applicability of CRISPR-engineered armored

CART cells. **a-c.** Anti-LeY CAR T cells derived from patients with multiple myeloma were engineered to express *Gfp* from either the *NR4A2* or *RGS16* locus and cocultured with OVCAR-3 tumor cells for 72 h before GFP expression was assessed. **a.** Flow cytometry plots from concatenated technical triplicates. **b.** Quantification of GFP percentage and **c.** MFI in CD8⁺ human CART T cells, represented as mean \pm SD of technical triplicates. **d.** Anti-LeY CAR T cells derived from patients with diffuse large B cell lymphoma were engineered to express IL-12 from the *NR4A2* locus and cocultured with OVCAR-3 or MCF-7 tumor cells for 24 h before cytokine concentration in supernatants was assessed. Concentrations of IFN γ , TNF or IL-2 produced by NR4A2/IL-12 CART T cells, represented as mean \pm SD of technical triplicates. **e-f.** Murine anti-hHer2 CAR T cells engineered to express *Gfp* from either the *Nr4a2* or *Rgs16* locus were cocultured with MC38 tumor cells with varying Her2 expression for 24 h before GFP expression was assessed. **e.** Histogram overlay showing Her2 expression in MC38 tumor cells. **f.** Quantification of GFP MFI in CD8⁺ murine CART T cells, represented as mean \pm SD of technical triplicates. **g-h.** Human anti-LeY CAR

T cells engineered to express *Gfp* from either the *NR4A2* or *RGS16* locus were stimulated with varying concentrations of anti-LeY idiotype antibody for 24 h before GFP and CD69 expression were assessed. **g.** Quantification of GFP MFI and **h.** CD69 percentage in CD8⁺ human CART T cells, represented as mean \pm SD of technical triplicates. **i-j.** Human anti-Her2 CAR T cells were engineered to express *Gfp* from the *NR4A2* locus and assessed in vitro upon stimulation with MDA-MB-231 tumor cells (**i**) and in mice bearing orthotopic MDA-MB-231 tumors (**j**). **i.** Flow cytometry plots from concatenated technical triplicates (left) and quantification of GFP expression represented as mean \pm SD of technical triplicates (right) in CD8⁺ human CART T cells post 24 h of stimulation. **j.** Flow cytometry plots representative of $n = 4$ mice/group in CD8⁺ human CART T cells 14 days post transfer. **k.** OT-3 T cells were engineered to express IL-12 or IL-2 from the *Nr4a2* or *Rgs16* locus, respectively, and cocultured with AT-3-ova tumor cells for 24 h before cytokine concentration in supernatants was assessed. Concentration of IL-12 (left) or IL-2 (right) produced by NR4A2/IL-12 or RGS16/IL-2 OT-3 T cells, respectively, represented as mean \pm SD of technical triplicates. **(b-d, f-g, i, k)** Two-way ANOVA. *n.s.* not significant, $***p < 0.0001$.

One-step manufacturing approach: *TRAC* knock-in of CAR



Extended Data Fig. 12 | One-step manufacturing approach for CRISPR-engineered armored CAR T cells. a-b. a-b. Anti-LeY CAR T cells manufactured via retroviral transduction or CRISPR-mediated knock-in to the *TRAC* locus were engineered to express *Gfp* from either the *NR4A2* or *RGS16* locus. a. Flow cytometry plots from concatenated technical triplicates (left) and quantification of CAR expression represented as mean \pm SD of technical triplicates (right) in CD8⁺ human CAR T cells. b. Quantification of GFP expression in CD8⁺ human CAR T cells upon in vitro stimulation with anti-LeY idiotype antibody, MCF-7 or

OVCAR-3 tumor cells for 24 h, represented as mean \pm SD of technical triplicates. **c-d.** Anti-LeY CAR T cells manufactured via CRISPR-mediated knock-in to the *TRAC* locus were engineered to express IL-12 or IL-2 from the *NR4A2* or *RGS16* locus, respectively, and assessed upon in vitro stimulation as per (b). **c.** Concentration of IL-12 or **d.** IL-2 produced by NR4A2/IL-12 or RGS16/IL-2 CAR T cells, respectively, represented as mean \pm SD of technical triplicates. **(c-d)** Two-way ANOVA. ** p $<$ 0.01, *** p $<$ 0.001, **** p $<$ 0.0001.

Reporting Summary

Nature Portfolio wishes to improve the reproducibility of the work that we publish. This form provides structure for consistency and transparency in reporting. For further information on Nature Portfolio policies, see our [Editorial Policies](#) and the [Editorial Policy Checklist](#).

Please do not complete any field with "not applicable" or n/a. Refer to the help text for what text to use if an item is not relevant to your study. [For final submission](#): please carefully check your responses for accuracy; you will not be able to make changes later.

Statistics

For all statistical analyses, confirm that the following items are present in the figure legend, table legend, main text, or Methods section.

n/a Confirmed

- The exact sample size (n) for each experimental group/condition, given as a discrete number and unit of measurement
- A statement on whether measurements were taken from distinct samples or whether the same sample was measured repeatedly
- The statistical test(s) used AND whether they are one- or two-sided
Only common tests should be described solely by name; describe more complex techniques in the Methods section.
- A description of all covariates tested
- A description of any assumptions or corrections, such as tests of normality and adjustment for multiple comparisons
- A full description of the statistical parameters including central tendency (e.g. means) or other basic estimates (e.g. regression coefficient) AND variation (e.g. standard deviation) or associated estimates of uncertainty (e.g. confidence intervals)
- For null hypothesis testing, the test statistic (e.g. F , t , r) with confidence intervals, effect sizes, degrees of freedom and P value noted
Give P values as exact values whenever suitable.
- For Bayesian analysis, information on the choice of priors and Markov chain Monte Carlo settings
- For hierarchical and complex designs, identification of the appropriate level for tests and full reporting of outcomes
- Estimates of effect sizes (e.g. Cohen's d , Pearson's r), indicating how they were calculated

Our web collection on [statistics for biologists](#) contains articles on many of the points above.

Software and code

Policy information about [availability of computer code](#)

Data collection Flow cytometry: BD FacsDiva version 8 (FlowJo LLC)
RNA-seq: CASAVA v1.8.2, Cutadapt v2.1, FastQC v0.11.6, RNA-SeQC v1.1.8

Data analysis Flow cytometry: FlowJo version 10 (FlowJo LLC)
Differentially expressed gene analysis: EdgeR (<https://bioconductor.org/packages/release/bioc/html/edgeR.html>)
General: Microsoft Excel 2010
Statistical analysis and data presentation: Graphpad Prism 9
Gene expression analysis: featureCounts, Rsubread 2.10.5

For manuscripts utilizing custom algorithms or software that are central to the research but not yet described in published literature, software must be made available to editors and reviewers. We strongly encourage code deposition in a community repository (e.g. GitHub). See the Nature Portfolio [guidelines for submitting code & software](#) for further information.

Data

Policy information about [availability of data](#)

All manuscripts must include a [data availability statement](#). This statement should provide the following information, where applicable:

- Accession codes, unique identifiers, or web links for publicly available datasets
- A description of any restrictions on data availability
- For clinical datasets or third party data, please ensure that the statement adheres to our [policy](#)

Data availability statement has been provided in the manuscript including accession codes.

Human research participants

Policy information about [studies involving human research participants and Sex and Gender in Research](#).

Reporting on sex and gender	N/A
Population characteristics	Patients had diffuse large B cell lymphoma or multiple myeloma.
Recruitment	<i>Describe how participants were recruited. Outline any potential self-selection bias or other biases that may be present and how these are likely to impact results.</i>
Ethics oversight	Ethics (HREC/74245/PMCC) for the study was approved by the Peter MacCallum Cancer Centre Human Research Ethics committee.

Note that full information on the approval of the study protocol must also be provided in the manuscript.

Field-specific reporting

Please select the one below that is the best fit for your research. If you are not sure, read the appropriate sections before making your selection.

Life sciences

Behavioural & social sciences

Ecological, evolutionary & environmental sciences

Life sciences study design

All studies must disclose on these points even when the disclosure is negative.

Sample size	Experiments were performed with sufficient power to achieve statistical significance based upon an effect size of 30%, which would have been deemed clinically significant. All therapeutic experiments were performed with a minimum of 3 mice per group.
Data exclusions	No data were excluded from the manuscript.
Replication	Unless otherwise stated, all experiments were replicated in at least 2 independent experiments.
Randomization	Mice were randomized prior to treatment according to tumor size to ensure all groups had equivalent tumor burden prior to therapy. Groups were age and sex matched.
Blinding	Data was not blinded. Investigators performed, acquired and analyzed all experiments.

Reporting for specific materials, systems and methods

We require information from authors about some types of materials, experimental systems and methods used in many studies. Here, indicate whether each material, system or method listed is relevant to your study. If you are not sure if a list item applies to your research, read the appropriate section before selecting a response.

Materials & experimental systems

n/a	Involved in the study
<input type="checkbox"/>	Antibodies
<input checked="" type="checkbox"/>	Eukaryotic cell lines
<input checked="" type="checkbox"/>	Palaeontology and archaeology
<input type="checkbox"/>	Animals and other organisms
<input checked="" type="checkbox"/>	Clinical data
<input checked="" type="checkbox"/>	Dual use research of concern

Methods

n/a	Involved in the study
<input checked="" type="checkbox"/>	ChIP-seq
<input type="checkbox"/>	Flow cytometry
<input checked="" type="checkbox"/>	MRI-based neuroimaging

Antibodies

Antibodies used	All antibodies used in the study were obtained from commercial suppliers (BD Pharmigen, Cell Signaling, eBioscience, Invitrogen, Thermo Scientific or Biologend).
Validation	All antibodies were validated by the supplier.

Eukaryotic cell lines

Policy information about [cell lines and Sex and Gender in Research](#)

Cell line source(s)	The murine breast carcinoma cell line AT-3-ova was generated from cells obtained from Dr. Trina Stewart (PMCC, Melbourne, Victoria, Australia). The murine colon adenocarcinoma MC38-hHer2 and MC38-ova cell lines and the 24JK-hHer2 cell line were generated from cells obtained from Dr. Jeff Schlom (National Institute of Health, Maryland, USA). The mouse breast carcinoma E0771-hHer2 and E0771-ova cell line were generated from cells obtained from Prof. Robin Anderson (Olivia Newton-John Cancer Centre, Victoria, Australia). OVCAR-3, MCF-7 and MDA-MB-231 tumor cell lines and GP+e86 and PG13 packaging lines were obtained from the American Type Culture Collection.
Authentication	Cell lines were not authenticated but were utilized within 10 passages of a master stock
Mycoplasma contamination	All lines were tested negative for mycoplasma contamination
Commonly misidentified lines (See ICLAC register)	None of the cell lines are listed on the ICLAC database

Animals and other research organisms

Policy information about [studies involving animals; ARRIVE guidelines](#) recommended for reporting animal research, and [Sex and Gender in Research](#)

Laboratory animals	C57BL/6 mice, NSG and transgenic mice were utilized where indicated. Mice were used between 6-16 weeks of age.
Wild animals	This study did not involve wild animals.
Reporting on sex	Studies utilizing AT3-ova, MC38-ova, E0771-hHer2, OVCAR-3 and MDA-MB-231 cells were performed in female mice. Studies using MC38-ova and MC38-hHer2 were performed in male mice.
Field-collected samples	N/A
Ethics oversight	Ethics oversight was performed by the Peter MacCallum Cancer Centre Animal Experimentation Ethics Committee (AEEC).

Note that full information on the approval of the study protocol must also be provided in the manuscript.

Flow Cytometry

Plots

Confirm that:

- The axis labels state the marker and fluorochrome used (e.g. CD4-FITC).
- The axis scales are clearly visible. Include numbers along axes only for bottom left plot of group (a 'group' is an analysis of identical markers).
- All plots are contour plots with outliers or pseudocolor plots.
- A numerical value for number of cells or percentage (with statistics) is provided.

Methodology

Sample preparation	Blood was collected via submandibular or retroorbital bleed into tubes containing EDTA prior to euthanasia. Blood and spleen samples were treated twice or once respectively with ACK lysis buffer before staining for flow cytometry. Tumors were digested in SAFC DMEM media with 0.01 mg/mL DNase (Sigma Aldrich) and 1 mg/mL type IV collagenase for 30 minutes at 37°C. Following digestion, tumor samples were filtered twice through a 70 µm filter to create a single cell suspension and resuspended in Fc block prior to staining for analysis by flow cytometry.
Instrument	FACS data were obtained on a BD FACSCanto II, LSRFortessa X-20, LSR II, FACSsymphony A3 or A5 from the Peter MacCallum Cancer Centre flow cytometry core facility.
Software	Data was analyzed using Flowjo software 10.8.1
Cell population abundance	N/A
Gating strategy	FSC/SSC gate was first used to gate on the morphology of leukocytes. A singlet gates was next used (FSC-A vs FSC-H) to exclude doublets followed by a viability gate (Fixable Yellow) to exclude dead cells. CAR T cells were identified using a T cell lineage marker (Thy1.2) and transduction marker (NGFR or FLAG).

Tick this box to confirm that a figure exemplifying the gating strategy is provided in the Supplementary Information.

